# Five Planets Orbiting 55 Cancri[1]

Debra A. Fischer[2], Geoffrey W. Marcy[3], R. Paul Butler[4], Steven S. Vogt[5], Greg Laughlin[5],
Gregory W. Henry[6], David Abouav[2], Kathryn M. G. Peek[3], Jason T. Wright[3], John A.
Johnson[3], Chris McCarthy[2], Howard Isaacson[2]

fischer@stars.sfsu.edu

## ABSTRACT

We report 18 years of Doppler shift measurements of a nearby star, 55 Cancri, that exhibit strong evidence for five orbiting planets. The four previously reported planets are strongly confirmed here. A fifth planet is presented, with an apparent orbital period of 260 days, placing it 0.78 AU from the star in the large empty zone between two other planets. The velocity wobble amplitude of 4.9 m s$^{-1}$ implies a minimum planet mass $M \sin i = 45.7$ M$_{\text{Earth}}$. The orbital eccentricity is consistent with a circular orbit, but modest eccentricity solutions give similar $\chi_{\nu}^2$ fits. All five planets reside in low eccentricity orbits, four having eccentricities under 0.1. The outermost planet orbits 5.8 AU from the star and has a minimum mass, $M \sin i = 3.8$ M$_{\text{Jup}}$, making it more massive than the inner four planets combined. Its orbital distance is the largest for an exoplanet with a well defined orbit. The innermost planet has a semi-major axis of only 0.038 AU and has a minimum mass, $M \sin i$, of only 10.8 M$_{\text{Earth}}$, one of the lowest mass exoplanets known. The five known planets within 6 AU define a *minimum mass*

*protoplanetary nebula* to compare with the classical minimum mass solar nebula. Numerical N-body simulations show this system of five planets to be dynamically stable and show that the planets with periods of 14.65 and 44.3 d are not in a mean-motion resonance. Millimagnitude photometry during 11 years reveals no brightness variations at any of the radial velocity periods, providing support for their interpretation as planetary.

*Subject headings:* planetary systems – stars: individual (HD 75732, $\rho^1$ Cancri, 55 Cancri)

## 1. Introduction

One of the first few detected exoplanets was a planetary companion to 55 Cnc (Butler et al. 1997). At the time, eight years of Doppler measurements from Lick Observatory revealed a 14.6-day wobble in 55 Cnc as it was gravitationally perturbed by a Jupiter-mass planet. Superimposed on this 14.6-day Doppler periodicity was an additional trend showing clear curvature and indicating that 55 Cancri was host to a second orbiting body, likely of planetary mass.

Additional Doppler measurements through 2002 uncovered the full Doppler cycle with a period of ∼14 yr, caused by a planet with a minimum mass $M \sin i = 4$ $M_{\mathrm{Jup}}$ orbiting ∼5.5 AU from 55 Cnc (Marcy et al. 2002). This was the first giant planet found with an orbital radius similar to the giant planets in our solar system. A third Doppler periodicity of 44.3 days was also apparent in those data, indicating a third Jupiter-mass planet in the system, this one orbiting 0.25 AU from the star (Marcy et al. 2002). This was the second planetary system found to have three planets, the first being that around $\upsilon$ Andromedae (Butler et al. 1999).

By combining these velocities from Lick Observatory with over 100 precise Doppler measurements obtained in one year at the Hobby-Eberly Telescope, along with measurements from the "Elodie" spectrometer at Haute Provence, McArthur et al. (2004) identified a fourth planet having a small minimum mass of $M \sin i = 14$ $M_{\mathrm{Earth}}$ with an orbital period of 2.8 d. This planet was one of the first three Neptune-mass planets discovered, along with the planets orbiting GJ 436 (Butler et al. 2004; Maness et al. 2007) and $\mu$ Arae (Santos et al. 2004). The detection of this Neptune-mass planet made 55 Cancri the first system known to contain four planets. McArthur et al. (2004) also used the Fine Guidance Sensor on the Hubble Space Telescope to carry out astrometry of 55 Cnc, and estimated the inclination of the orbital plane of the outer planet to be $i = 53 \pm 6.8$ deg.

This four-planet system left a large, dynamically empty gap between 0.25 and 6 AU. Numerical simulations suggested that hypothetical planets in this gap would be dynamically stable, including the interesting possibility of terrestrial mass planets in the habitable zone between 0.5 and ~2 AU (Marcy et al. 2002; Raymond, Barnes, & Kaib 2006).

In 2004, we noticed modest peaks in the periodogram at 260 and 470 d, indicating possible planets at those periods that motivated our continued intense Doppler observations. Wisdom (2005) carried out an independent analysis of the combined published Doppler measurements and suggested that the 2.8 d periodicity was possibly an alias rather than caused by a planet, putting the existence of the 2.8 d planet in question. He also identified a 260 d periodicity, implying a new planet with a minimum mass of 1.8 $M_{Nep}$ = 31 $M_{Earth}$. It is not uncommon for modest peaks in the periodogram to fluctuate in their confidence level with the addition of new data, especially for cases where the radial velocity amplitudes are comparable to the precision of Doppler measurements, so we intensified our observations of this star. Here, we add 115 additional radial velocity measurements from Lick Observatory and 70 radial velocity measurements from Keck Observatory to our previous data set and find that the false alarm probability for a 260-d signal has strengthened and is present in data sets from both Observatories independently.

A stellar companion orbits 55 Cancri as well. It is a 13th magnitude M dwarf located roughly 1000 AU away, certainly bound to 55 Cancri A as the radial velocities are nearly the same. The occurrence, dynamics, and final properties of planetary systems may well be affected by such stellar companions, as indicated in observational studies by Eggenberger, Udry, & Mayor (2004) and Raghavan et al. (2006). Thus 55 Cancri offers a test of the effects of binary companions on the architecture of complex planetary systems.

Spitzer Space Telescope results for 55 Cnc by Bryden et al. (2006) show that the observed 24 and 70 micron flux densities are comparable to the predicted brightness of the stellar photosphere, indicating no infrared excess above the errors. The corresponding upper limit to the fractional infrared luminosity is $8 \times 10^{-6}$, or about 80 zodis. A detectable scattered light disk was also ruled out by its non-detection in HST NICMOS data by Schneider et al. (2001).

Here we provide Doppler measurements from both Lick and Keck Observatories that significantly augment the 2002 set from Lick Observatory alone. These measurements span a longer time baseline and contain higher Doppler precision with the addition of new Keck velocities, offering a chance to reassess all of the planets around 55 Cancri.

## 2. Properties of 55 Cancri

55 Cnc (=HD 75732=$\rho^1$ Cnc A = HR3522=HIP 43587) has an apparent brightness $V = 5.96$ and Hipparcos parallax of $79.8 \pm 0.84$ mas (ESA 1997), implying a distance of $12.5 \pm 0.13$ parsecs and absolute visual magnitude $M_V = 5.47$. Using spectra from the California & Carnegie Planet Search, Valenti & Fischer (2005) derived $T_{eff} = 5234 \pm 30$K, $\log g = 4.45 \pm 0.08$, $v \sin i = 2.4 \pm 0.5$km s$^{-1}$ , and [Fe/H]= $+0.31 \pm 0.04$. Indeed, 55 Cnc is so metal-rich as to be in the fifth metallicity percentile of stars within 25 pc (Valenti & Fischer 2005). Using a bolometric correction that accounts for the high metallicity (VandenBerg & Clem 2003), we calculate a stellar luminosity of 0.6 L$_\odot$. The effective temperature, spectroscopic surface gravity and intrinsic luminosity are all consistent with a spectral classification of this star as K0/G8V. The star is chromospherically inactive, with a Mt. Wilson $S$-value of 0.22 (averaged during the past seven years of our measurements) implying $\log R'_{\rm HK} = -4.84$, indicating a modest age of 2-8 Gyr where 2 Gyr is a strong lower limit on age. The rotation period, calibrated to this chromospheric activity, is estimated to be 39 days (Noyes et al. 1984; Wright et al. 2004). However, for metal-rich stars, chromospheric emission at the Ca II H & K lines remain poorly calibrated as a diagnostic of rotation and age. A more complete discussion of the chromospheric activity and implied stellar properties are given by Marcy et al. (2002).

The mass of 55 Cnc is best determined by associating its measured effective temperature, luminosity, and metallicity with models of stellar interiors. Using the well known "Yale models," (Yi, Demarque, & Kim 2004), Valenti & Fischer (2005) found a stellar mass of $0.92 \pm 0.05$ M$_\odot$. Takeda et al. (2007) have also derived modified stellar evolutionary models using the Yale Stellar Evolution Code to match the observed spectroscopic parameters from Valenti & Fischer (2005). They derive a stellar mass for 55 Cnc of $0.96 \pm 0.05$ M$_\odot$ with the uncertainty corresponding to the 99.7% credibility intervals of the Bayesian posterior probability distributions. Here we simply adopt the average of these two estimates, giving $M = 0.94 \pm 0.05$ M$_\odot$ for the mass of 55 Cnc. We note that the adopted uncertainty in stellar mass implies fractional errors in the derived planetary masses of 8 percent in addition to errors in the orbital parameters.

## 3. Doppler–Shift Measurements

We have obtained 636 observations of the G8 main-sequence star 55 Cnc over the past 18 years. We generally obtain two or three consecutive observations and bin them to increase the velocity precision and accuracy. Here, we present 250 binned velocity measurements made at Lick Observatory from 1989-2007, and 70 binned velocity measurements made at the

Keck Observatory from 2002–2007. The Lick spectra were obtained using both the 3-meter telescope and the Coudé Auxiliary Telescope, which both feed the Hamilton optical echelle spectrometer (Vogt 1987). A detailed description of the setup of the Hamilton spectrometer, its calibrating iodine absorption cell, and the method of extracting Doppler measurements for 55 Cnc are given in Butler et al. (1996) and in Marcy et al. (2002). The Keck spectra were obtained with the HIRES spectrometer (Vogt et al. 1994), and a description of that setup and Doppler measurements are given in Butler et al. (2006).

At both telescopes, we place a cylindrical, pyrex cell filled with molecular iodine gas in the light path of the telescope, just before the spectrometer slit, to superimpose sharp absorption lines of known wavelength on the stellar spectrum. The iodine lines provide calibration of both wavelength and the spectrometer PSF (Butler et al 1996). While twenty percent of the starlight is absorbed by iodine, the cell's inclusion is worthwhile because the dense iodine absorption lines provide a permanent record of the wavelength scale and behavior of the spectrometer at the instant of each observation, producing long-term Doppler precision free of systematic errors to the level of 1 m s$^{-1}$.

The velocity measurements are listed in Table 1 (the full Table is available in the electronic version of this paper only) and shown in Figure 1 with different symbols for measurements made at Lick and Keck. We carried out a preliminary five-Keplerian fit to the combined velocities from both telescopes, allowing one extra parameter to be the difference in the velocity zero-point from the two spectrometers, found to be $28.8 \pm 0.5$ m s$^{-1}$. Once established, we applied the $+28.8$ m s$^{-1}$ correction to the Keck data, putting the two spectrometers' measurements on the same velocity scale before showing them in Figure 1 and listing them in Table 1. The first 14 Doppler measurements made between 1989 and November 1994 typically have uncertainties of 8–10 m s$^{-1}$, worse than most of the subsequent observations due to the unrepaired optics of the Hamilton spectrometer. Observations made at Lick since December 1994 have typical uncertainties of 3–5 m s$^{-1}$. At Keck, between 1999 and 2004, the typical Doppler uncertainty is 3 m s$^{-1}$. In August 2004 the optics and CCD detector for HIRES were upgraded, reducing the Doppler errors. In November 2004 we began making three consecutive observations (and sometimes five) of 55 Cnc to average over stellar p-mode oscillations that can add 1 m s$^{-1}$ velocity noise to G8V main sequence stars (Kjeldsen et al. 2005). The resulting Doppler precision at Keck since August 2004 has been 1.0–1.5 m s$^{-1}$.

## 4. Keplerian Fits to Doppler Measurements

The Doppler measurements of 55 Cnc were fit with a series of Keplerian models, each model having an increasing number of planets, beginning with the two well established periods of 14.65 d and 14.7 yr (Marcy et al. 2002). We polished all models with a Marquardt minimization of $\chi^2_\nu$ to establish the best-fit model. The weights assigned to each Doppler measurement are the inverse square of each measurement's uncertainty, which are approximated as the quadrature sum of the internal uncertainty in the Doppler measurement and the "jitter" that stems from photospheric motions and instrumental errors (Wright 2005). Experience with similar G8 main-sequence stars suggests that the combined astrophysical and instrumental jitter is 3 m s$^{-1}$ at Lick and 1.5 m s$^{-1}$ at Keck, both values being uncertain by 50 percent. The jitter prediction is complicated by the high metallicity of 55 Cnc, [Fe/H] = +0.3. The radiative transfer of Ca II H & K in 55 Cnc will be different from that in solar metallicity stars, because of higher line and continuous opacities, rendering the calibration of emission with stellar age, rotation, and jitter even more uncertain. However, the estimated rotation period of 39 d from periodicities in the Ca II H & K emission and the star's low rotational $v \sin i$ of 2.5 km s$^{-1}$ confirm that the star has, at most, a modest level of magnetic activity, indicating correspondingly modest jitter with an upper limit of 4 m s$^{-1}$. For this analysis, we adopt a jitter value of 1.5 m s$^{-1}$ and 3.0 m s$^{-1}$ for Keck and Lick, respectively.

After fitting a model with the two well established planets, we assessed the statistical significance of any periodicities remaining in the residuals to motivate addition of another planet to the model, as described in detail below. We determine false alarm probabilities for peaks in the periodogram attributed to any additional planets by testing the null hypothesis that the current velocity residuals are merely incoherent noise. In such tests, the velocity residuals to our best-fit model are scrambled and their periodograms computed to assess the fraction of trials with scrambled residuals that have a stronger peaks. This FAP assessment makes few assumptions about the width or shape of the distribution of noise.

### 4.1. The Three-Planet Model

Our initial model consisted of the sum of two Keplerian orbits (no gravitational interactions) for the two planets having secure orbital periods of 14.65 d and ∼14.7 yr, both strongly supported by all of our past Doppler analyses of this star (Marcy et al. 2002). A two-planet fit yields periods of 14.65 d and 14.7 yr and eccentricities of 0.002 and 0.06 for the two planets, respectively. The residuals have an RMS of 11.28 m s$^{-1}$ and $\sqrt{\chi^2_\nu}$ of 3.42. An accurate model would have an RMS on the order of the errors in the data plus "jitter" (∼5 m s$^{-1}$) and $\sqrt{\chi^2_\nu}$ near 1. These large values of RMS and $\sqrt{\chi^2_\nu}$ indicate that the model

is inadequate. The periodogram of the residuals (Figure 2) exhibits a tall peak at a period of 44.3 d and power of 55, clearly significant above the noise. This period corresponds to the orbit of the planet suspected in Marcy et al. (2002). This 44.3 d period is most likely caused by a third planet as the only other explanation would be rotational variation from surface inhomogeneities. Such rotational explanations are ruled out both by the shorter stellar rotational period, 42.7 d, found in the photometry as shown in §6, and by the large velocity amplitude of 10.6 m s$^{-1}$, which is never seen in such chromospherically quiet stars. Furthermore, photospheric features generally only survive for a few rotation periods of the star. It seems unlikely that surface inhomogeneities would persist for more than a decade and maintain rotational phase coherence.

A Levenberg-Marquardt minimization was used to find the best-fit orbital parameters for a three-planet Keplerian model with periods near 14.65 d, 44.34 d, and 14.7 yr. The best fit yielded residuals with an RMS scatter of 8.62 m s$^{-1}$and $\sqrt{\chi^2_\nu} = 2.50$. This result represents an improved fit to the two-planet model, but is still clearly inadequate, not surprising as the model did not include a periodicity near 2.8 d as found by McArthur et al. (2004). Indeed, the periodogram of the residuals to the three-planet fit, shown in Figure 3, reveals two additional strong peaks near 2.8 d and 260 d.

## 4.2.   The Four-Planet Model

We proceeded to test a 4-planet model by including a fourth planet with a period near 2.8 d (McArthur et al. 2004). The best-fit 4-planet model gave periods of 2.81 d, 14.65184 d, 44.32 d, 14.4 yr, all with eccentricities less than 0.3. The residuals have RMS of 7.87 m s$^{-1}$ and $\sqrt{\chi^2_\nu} = 2.12$, both representing a significant improvement over the 3-planet model. (In computing both the RMS and $\chi^2_\nu$, the denominator was appropriately diminished by the greater number of free parameters, i.e., five per planet.) Thus both the periodogram in Figure 3 and the superior fit with four planets offer support for the existence of the planet with 2.81 d, corresponding to the planet with $P = 2.808 \pm 0.002$ d in McArthur et al. (2004).

However this 4-planet model remains inadequate for two reasons. The residuals reveal a poor fit with $\sqrt{\chi^2_\nu} = 2.12$ and an RMS of 7.87 m s$^{-1}$, larger than explainable by the Doppler errors and jitter. Also, a periodogram of the residuals reveals a peak at a period of 260.1 d, as shown in Figure 4, and some additional smaller peaks.

### 4.3.   Assessing the Periodicity near 260 d

The periodogram peak near 260 d (Figure 4) in the residuals to the 4-planet model could be spurious, caused by fluctuations arising from photon-limited Doppler errors in the spectra or by aliases in the window function of the sampling times. The CCD detector at Lick Observatory has been upgraded four times in the past eighteen years, which could produce discontinuities of 1–2 m s$^{-1}$ in their zero points and even create an alias. Such abrupt, one-time instrumental changes should not produce periodicities. Nonetheless, to check for such effects, the four-planet Keplerian model was fit separately to the Lick and Keck velocities.

The 250 velocities from Lick against only 70 from Keck cause the periodogram in Figure 4 to be heavily weighted toward the Lick measurements. The prominent period at 260 d certainly reflects the Lick velocities more than those from Keck, leaving open the question of independent confirmation of the 260 d period in the Keck data. We fit a 4-planet model to the 70 Keck velocities alone. The Keck velocities offer higher precision ($\sim$1.5 m s$^{-1}$ ) than those from Lick but carry the disadvantage of a duration of only 5 1/2 years.

The four-planet fit to the Keck velocities alone yielded residuals with RMS = 4.3 m s$^{-1}$ and $\sqrt{\chi^2_\nu}$ = 2.59. The periodogram of the residuals is shown in Figure 5, and it reveals a peak at a period of 266 d with a power of 7.7. There is no significant power at any other periods. The power in the 266 d peak is higher than all peaks for periods between 1-3000 d. Importantly, the peak at 266 d is roughly twice as high as the noise peaks. Although this peak is not overwhelming by itself, the independent occurrence of a periodicity near 265 d in the Keck velocities along with the similar period found in the Lick velocities, supports the reality of that period and argues against systematic errors as the cause.

One might be concerned that the Keck velocities yielded such a modest peak at $\sim$266 d (Figure 5) as compared to the relatively strong peak in the Lick data (Figure 4). We addressed this concern by augmenting the Keck velocities with artificial velocities corresponding to a planet having a period of 260 d in a Keplerian orbit that causes a semiamplitude of $K = 4.4$ m s$^{-1}$. The idea is that if the power in the periodogram doubles, then the modest peak in Figure 5 is probably reasonable. We performed a four-planet fit and computed the periodogram of the residuals. A peak at $P = 261$ d was seen with a power of 13, roughly double the power of the peak that emerged from the original velocities. Thus, the 266 d peak in the periodogram from the original Keck velocities (Figure 5) constitutes a confirmation of the $\sim$265 d planet seen in Figure 4 having that period and amplitude. Of course, the Lick velocities alone also exhibit the 260 d peak indepedently.

We also checked to see if the 260 d signal might be an alias of the possible 470 d peak seen in Figure 4. We fit the combined Lick and Keck velocities with a five-planet model

having a fifth planet with a period near 470 d instead of near 260 d. The periodogram of the residuals to this five-planet model still has a strong peak with period near 263 d, with a power of 19. Apparently the period at 260 d does not vanish by including a 470 d period in the model and thus is not an alias of it.

We assessed the probability that the 260 d signal was caused by chance fluctuations in the velocities by performing a conservative false alarm probability test. We fit the combined velocities with only a four-planet model and tested the null hypothesis that no periodicity near 260 d actually exists in the residuals, implying that the peak is due merely to noise. We scrambled the residuals to the four-planet fit but kept the times of observation the same, and recomputed the periodogram for each of 500 trials. We recorded the power of the tallest peak in the periodogram from each of 500 trials. The histogram of those peak powers is shown in Figure 6. The typical peaks from the scrambled residuals have powers of 7–13, with the tallest being 16. In contrast, the periodogram of the original residuals had a peak height of 31.5, shown both in 4 and as the vertical dashed line in 6. Thus, the null hypothesis (that the residuals have no coherence) is unlikely and the associated false alarm probability of the peak at 260 d is less than 0.002, indicating that the periodicity is real.

The analysis above strongly supports the existence of a planet with a period of 260 d. The period of 260 d does not correspond to any known time scale of stellar interiors or atmospheres, nor to the rotation period of the star which is 42.7 d (see below). Thus, a plausible interpretation is a planet with a period near $P = 260$ d, making it the fifth planet in the 55 Cnc system.

### 4.4. The Five-Planet Model with a 260-day Planet

We constructed a Keplerian model that included a fifth planet having a period near 260 d. A best-fit model to the combined Lick and Keck velocities was found easily, yielding five periods of 14.65162 d, 44.344 d, 5218 d, 2.817 d, and 260.0 d (see Table 2). The residuals have RMS = 6.74 m s$^{-1}$ and $\sqrt{\chi_\nu^2} = 1.67$ (including the jitter in the expected variance), and a periodogram of them is shown in Figure 7. The values of the RMS and $\sqrt{\chi_\nu^2}$ are 15% and 20% lower, respectively, than the corresponding diagnostics of the four-planet model. Table 3 gives the RMS and $\sqrt{\chi_\nu^2}$ for all multi-planet models considered in this paper, showing the significant improvement with each additional planet. This major improvement in the quality of the fit of 320 measurements, coming from a fifth planet with its five additional free parameters, indicates that the new model has considerable merit. The five-planet model containing the 260 d planet is clearly superior to the four-planet model. The period agrees with that found by Wisdom (2005) from a periodogram analysis of our earlier, published

velocities from Lick Observatory.

As this model contains a proposed planet with $P = 260$ d, we present in Table 2 all of the orbital parameters for all five planets self-consistently computed with a Levenberg-Marquardt least squares algorithm. Considerable trial and error with various starting guesses for the 26 free parameters was carried out to ensure that the least squares search began near the deepest minimum. The $\chi_\nu^2$ fit was virtually unchanged for orbital eccentricites between 0.0 to 0.4 for the 260 d planet. This is not surprising since the amplitude of the planet is comparable to the single measurement precision for most of our data. Although the orbit is consistent with circular, we adopted an intermediate eccentricity of $0.2 \pm 0.2$ to indicate the indistinguishable range of eccentricity. The best-fit parameters for the 260 d planet are $e = 0.2 \pm 0.2$, $K = 4.879 \pm 0.6$ m s$^{-1}$, implying $M \sin i = 0.144 \pm 0.04$ M$_{\rm Jup}$.

The innermost planet has $P = 2.81705 \pm 0.0001$ d, $e = 0.07 \pm 0.06$, $K = 5.07 \pm 0.53$ m s$^{-1}$, and $M \sin i = 0.034$ M$_{\rm Jup}$ = 10.8 M$_{\rm Earth}$. In comparison, McArthur et al. (2004) found the inner planet to have a period, $P = 2.808 \pm 0.002$ d, $e = 0.174 \pm 0.127$, $K = 6.67$ m s$^{-1}$, and $M \sin i = 0.045$ M$_{\rm Jup}$ = 14.2 M$_{\rm Earth}$.

There is no question that the planet with $P$=2.817 d is the planet previously identified as having a period of 2.808 d (McArthur et al. 2004). The new minimum mass $M \sin i = 10.8$ M$_{\rm Earth}$ is lower than the 14.2 M$_{\rm Earth}$ previously reported in McArthur et al.. These differences are not surprising as some of the excess velocity variation previously left to be absorbed by the four known planets is now accounted for by the fifth planet.

The phase-folded velocities for the 260-day planet are shown in Figure 8 after subtracting the sum of the computed velocities of the other four planets from the measured velocities. The orbital eccentricity has been fixed to 0.2. The resulting residual velocities are plotted versus orbital phase and shown in Figure 8. The residuals reveal the 260 d period that had been detected in the periodogram and the Keplerian model is overplotted. The scatter has an RMS of 6.74 m s$^{-1}$. The error bars shown in Figure 8 include the quadrature sum of the internal errors (typically 2 m s$^{-1}$ for Keck and 4 m s$^{-1}$ for Lick) and the "jitter" (1.5 m s$^{-1}$ for Keck and 3 m s$^{-1}$ for Lick). Thus, the scatter of 6.74 m s$^{-1}$ is only slightly larger than the known internal errors and expected jitter (astrophysical and instrumental).

## 5. Residual Planets

Several explanations for the modest 6.74 m s$^{-1}$ scatter in the residuals are possible. Perhaps we are underestimating our internal errors. Perhaps the jitter for this metal-rich star is somewhat higher than the average for G8 main-sequence stars. Or perhaps there

are other planets that cause a sufficiently low signal that they are not apparent in the periodograms but nonetheless add a few m s$^{-1}$ of "noise" to the velocities.

We assessed the detectability of a hypothetical 6th planet by adding the velocities that would be induced by it to the observed velocities. We fit a 5-planet model to these augmented velocities, allowing all 26 parameters to float. We searched the periodogram of the residuals for peaks that loom above those arising in the 5-planet fit of the actual velocities (Figure 7). Such peaks would have been identified as a candidate 6th planet. We considered orbital periods from 300 d - 4000 d and determined the minimum $M \sin i$ that produced a peak 50% above any of the peaks in the actual periodogram (i.e. above a power of 15).

The minimum detectable mass of a hypothetical 6th planet is a sensitive function of its period and phase as those parameters determine how easily the signal can be absorbed in the 5-planet model, avoiding detection. Neighboring periods differing by a mere few percent can produce periodogram peaks differing by a factor of two simply due to differing commensurability with the 5 existing planets. A 6th planet in a mean motion resonance is particularly capable of avoiding detection in the face of the five existing planets. Such fine structure aside, the simulations can be characterized as follows. For orbital periods of 300 - 850 d, a 6th planet with Msini below 50 $M_{\rm Earth}$ would have eluded detection as the periodogram peaks would not have loomed even 50% above the noise. For periods 850 d - 1500 d, a 6th planet could avoid detection by having $M \sin i$ below 100 $M_{\rm Earth}$. For periods 1750 - 4000 d, planets below 250 $M_{\rm Earth}$ would elude detection. Thus such planets could exist around 55 Cnc and yet have avoided detection by our current 18 years of Doppler measurements. Indeed several such planets could exist in the large gap between periods of 260 d and 13 yr and probably maintain dynamical stability.

## 6.  Dynamical Simulations of the Multi-Planet System

The models in this paper are based on the approximation that the planetary orbits are Keplerian ellipses. In actuality, the radial velocity variation of the parent star over nearly two decades of observation is also affected by the mutual gravitational perturbations between the planets. As a concrete example, one can interpret the 5-planet fit in Table 2 as describing a set of osculating orbital elements at the epoch JD 2447578.730 of the first radial velocity observation. By making a choice of epoch, one creates a unique initial condition for a six-body integration of Newton's equations of motion. When this integration is carried out, one finds radial velocity deviations of $\Delta V > 25$ m s$^{-1}$ in comparing Keplerian and Newtonian models at epochs near JD 2454000.

These deviations arise primarily from the orbital precessions of planets b, c, and d that occur in the Newtonian model that are absent from the Keplerian model. Because the orbits are nearly circular, a Keplerian 5-planet fit can, however, compensate for nearly all of the precession through small adjustments to the orbital periods.

It is likely that one can obtain an improved chi-square by adopting a self-consistent N-body model for the stellar reflex velocity (e.g. Rivera et al. 2005). In addition to lowering the RMS of the fit, a definitive model of this type allows for the correct characterization of the possible 3:1 resonant relationship between planets b and c, and can therefore give important clues to the formation history of the system. Adopting the Keplerian fit in Table 2 as an intial guess, we used Levenberg-Marquardt minimization to obtain a self-consistent 5-planet dynamical fit to the radial velocity data sets. The resulting orbital parameters of our dynamical fit are all quite similar to their corresponding values in the Keplerian model, and are listed in Table 4. Our dynamical fit has $\sqrt{\chi^2}$=2.012 (without including any jitter), and RMS=7.712 m s$^{-1}$ . A more computationally expensive search should be able to find orbital parameters that provide a slight improvement to these values. We leave such an analysis to future work.

In order to assess the dynamical stability of our five-planet model, we adopt the self-consistent orbital elements in Table 4 and integrate the system forward for one million years from epoch JD 2447578.730. We used a Bulirsch-Stoer integrator (Press et al. 1992). The system remained stable throughout a one million year integration. The evolution of the five planetary eccentricities during a representative $2.5 \times 10^4$ year interval are shown in Figure 10. As is true throughout the $10^6$ year integration, the eccentricity variations experienced by all five planets are quite modest, and the system appears likely to be dynamically stable for long periods.

It is interesting to note that during the course of the numerical integration, the 3:1 resonant arguments for planets b and c are all circulating. This indicates that planets "b" and "c" do not currently participate in a low-order mean motion resonance, despite the near commensurability of their orbital periods.

We have computed the eccentricity variations that result when the system is modeled using a secular perturbation theory that includes terms up to second order in eccentricity (see, e.g., Murray & Dermott 1999), and which includes the leading-order effects of general relativity as outlined by Adams & Laughlin (2006). The results are quite similar to those in Figure 10. This indicates that the bulk of the planet-planet interactions in the system can be accounted for with a simple second-order theory, thus improving the likelihood that the configuration of planets can remain dynamically stable for the lifetime of the star.

## 7. Photometry of 55 Cancri

We have used the T8 0.8 m automatic photometric telescope (APT) at Fairborn Observatory to obtain high-precision photometry of 55 Cnc during 11 observing seasons between 1996 November and 2007 April. The T8 APT is one of several automated telescopes at Fairborn dedicated to observing long-term, low-amplitude brightness variations in solar-type stars associated with stellar magnetic cycles as well as to measuring short-term, low-amplitude variations caused by rotational modulation in the visibility of surface magnetic features (Henry 1999). APT photometry of planetary candidate stars helps to establish whether observed radial velocity variations are caused by stellar activity or planetary-reflex motion, and direct measures of stellar rotation periods provide good age estimates of the planetary systems (e.g., Henry et al. 2000). Queloz et al. (2001) and Paulson et al. (2004) have published several examples of periodic radial velocity variations in solar-type stars caused by photospheric spots and plages. The APT observations are also useful to search for transits of the planetary companions. The rare transiting systems allow direct determination of basic planetary parameters such as mass, radius, and mean density and so provide observational constraints on models of planetary composition and internal structure (e.g., Sato et al. 2005). Bright transiting systems enable detailed follow-up studies of exoplanet atmospheres (e.g., Richardson et al. 2007). Finally, monitoring a planetary host star's long-term luminosity variations provides a measure of the star's climate forcing ability on its system of planets (e.g., Hall, Henry, & Lockwood 2007).

The T8 APT is equipped with a two-channel precision photometer employing two EMI 9124QB bi-alkali photomultiplier tubes to make simultaneous measurements in the Strömgren $b$ and $y$ pass bands. The APT measures the difference in brightness between a program star and one or more nearby constant comparison star(s); the primary comparison star used for 55 Cnc is HD 76572 ($V = 6.28$, $B - V = 0.42$, F6 IV-V). The Strömgren $b$ and $y$ differential magnitudes are corrected for differential extinction with nightly extinction coefficients and transformed to the Strömgren system with yearly mean transformation coefficients. Finally, the $\Delta b$ and $\Delta y$ observations are combined into a single $\Delta(b + y)/2$ pass band to increase the photometric precision. The external precision of a single differential magnitude is typically around 0.0015 mag for the T8 APT, as determined from pairs of constant stars. Further details on the telescope, photometer, observing procedures, and data reduction techniques can be found in Henry (1999).

The complete 11-yr set of differential magnitudes computed with the primary comparison star is plotted in the top panel of Figure 11. Intercomparison of the primary comparison star with two secondary comparisons (HD 77190, $V = 6.07$, $B - V = 0.24$, A8Vn; HD 79929, $V = 6.77$, $B - V = 0.41$, F6V) revealed that the annual means of the primary compari-

son vary over a range of 0.003 mag from year to year. Rather than switch to one of the more stable secondary comparison stars, we have instead normalized the 11 seasons with the primary comparison so they all have the same annual mean. This was done because the secondary comparison stars have been used only for the past seven years. The normalization removes any long-term variation in the primary comparison star as well as in 55 Cnc, but this improves the sensitivity of our transit search described below for orbital periods under one year. After normalization, outliers exceeding three standard deviations were removed. The final data set in the top panel of Figure 11 contains 1349 nightly observations; the standard deviation of an individual observation from the normalized mean is 0.0017 mag.

The 0.0017 mag standard deviation of the full data set is only slightly greater than the nominal measurement precision of 0.0015 mag but suggests that low-amplitude, short-term intrinsic variability might be present at times in 55 Cnc. (Long-term variability has been removed by the normalization). We searched each annual set of measurements for evidence of coherent, low-amplitude variability that might be the result of rotational modulation in the visibility of starspots. The middle panel of Figure 11, which shows photometry from a portion of the 9th observing season, exhibits the clearest example of coherent variability in the data set. Two cycles of brightness variation are visible with an amplitude of approximately 0.006 mag. We interpret this as evidence for a small starspot region (covering less than 1% of the star's visible surface) that has survived for two rotation cycles of the star. A power spectrum of the observations in the middle panel is computed with the method of Vaníček (1971) and shown in the bottom panel of Figure 11. This gives a period of $42.7 \pm 2.5$ days, which we interpret to be the stellar rotation period. This confirms the rotation period of 55 Cnc reported by Henry et al. (2000), who used rotational modulation of the Ca II H & K flux measured by the HK Project at Mount Wilson Observatory (Baliunas et al. 1998).

We searched the photometric data for evidence of transits of the four inner planets; the results are summarized in Table 4 and plotted in Figure 12. We first computed the semi-amplitudes of the light curves (column 3) with least-squares sine fits of the complete data set phased to the four shortest radial velocity periods. The resulting amplitudes are all extremely small and consistent with zero. These very tight limits on photometric variability on the radial velocity periods clearly support planetary-reflex motion as the cause of the radial velocity variations. While our measured 42.7 day rotation period is consistent with the 44.35 day radial velocity period because of the relatively large uncertainty of 2.5 days in the rotation period, the absence of any photometric variability on the more accurate 44.35 day radial velocity period is strong support for the existence of 55 Cnc c.

In Figure 12, we have plotted light curves of the photometric data phased with the orbital periods of the inner four planetary companions. Zero phase in each panel represents

the predicted phase of mid transit for each of the companions. Only phases from 0.94 to 0.06 are plotted to improve visibility of any possible transits. The solid curve in each panel approximates the predicted transit light curve, assuming a planetary orbital inclination of 90°(central transits). The out-of-transit light level corresponds to the mean (normalized) brightness of the observations. The transit durations are calculated from the orbital elements, while the transit depths are derived from the estimated stellar radii and the planetary radii computed with the models of Bodenheimer, Laughlin, & Lin (2003). The horizontal error bar below each predicted transit curve represents the approximate $\pm 1\sigma$ uncertainty in the time of mid transit, based on Monte Carlo simulations and the uncertainties in the orbital elements. The vertical error bar represents the typical $\pm 0.0015$ mag uncertainty of a single observation.

Column 4 of Table 5 lists the geometric probability of transits for each of the five companions, computed from equation 1 of Seagroves et al. (2003) and assuming random orbital inclinations. The predicted transit depths for each planet determined as described above are given in Column 5, and the "observed transit depths" are recorded in column 6. The observed depths are computed as the difference in the mean light levels between observations that fall inside and outside of the transit windows plotted in Figure 12; a positive depth indicates a brightness drop in the transit window.

Unfortunately, we see no evidence for transits of the inner, low-mass companion 55 Cnc e; the mean of the 51 observations within its predicted transit window agree with the out-of-transit observations within $0.00029\pm0.0002$ mag, a result consistent with the absence of 0.00065 mag transits but still allowing a small possibility for their existence. Since the uncertainty in the time of mid transit is rather large compared to the transit duration, we searched for shallow transits over the full range of phases and over orbital periods between 2.70–2.90 days with null results. The secure detection of transits of such a small body would require reducing the uncertainty of the in-transit brightness mean by a factor of about two, which would require a factor of four more observations. This could be accomplished with the APT over the next observing season or two by concentrating brightness measurements around the times of predicted transits. We are forced to leave our non-detection of transits of 55 Cnc e as an uncertain result, as indicated by the colon in column 7 of Table 5.

Table 5 and Figure 12 demonstrate that transits with the expected depths of 55 Cnc b and 55 Cnc c do not occur. The observed transit depths are both consistent with zero. Figure 12 shows that we have no photometric observations during the predicted time of transit of 55 Cnc f. However, given the uncertainty in the transit timing and the density of observations within the uncertainty range, we conclude that transits of planet f probably do not occur. We have insufficient radial velocities to predict accurate transit times of the

outermost planet 55 Cnc d, so we can say nothing about their occurrence. We note that our non-detection of transits is consistent with the likely inclinations of the planetary orbits as discussed in §7 (below).

Finally, we comment on the long-term variability of the host star 55 Cnc. Although our normalization of the light curve has removed any such variation from the present analysis, an examination of the light curves computed with the secondary comparison stars mentioned above show that 55 Cnc clearly exhibits year-to-year variations in mean brightness with an amplitude of 0.001 mag over a time scale of several years or more (Henry et al.,in preparation). Thus, long- and short-term brightness variations in 55 Cnc are very similar to irradiance variations in our Sun (.e.g., Willson 1977).

## 8.    Minimum Mass Protoplanetary Nebula

Planet formation in the protoplanetary disk around 55 Cnc was apparently extraordinarily efficient, yielding at least five planets. Our extensive radial velocity data set, with its 18-year baseline, gives no indication that additional Jupiter-mass companions exist beyond 6 AU, although Saturn-mass or smaller planets would easily go undetected. If, as a thought experiment, we grind up the currently known planets, we may infer the properties of the protoplanetary disk around 55 Cnc.

We first assume an edge-on, co-planar geometry with $i = 90°$, and *in situ* formation of the planets directly from the disk gas, e.g. Boss (1997). In this case, the masses of planets total $\sim 5.3 M_{\rm Jup}$ and together imply a lower limit of 410 g cm$^{-2}$ for the average surface density of the disk interior to 6 AU. For a gas-to-dust ratio of 100, this implies an average surface density in solids of 4 g cm$^{-2}$. If the radial surface density profile of 55 Cancri's protostellar disk declined as $\sigma(r) \propto r^{-3/2}$, this implies a solid surface density of 1.4 g cm$^{-2}$ at 5 AU, which is approximately half the value of the minimum-mass solar nebula at Jupiter's current position.

In all likelihood, however, the surface density of solids in 55 Cancri's protostellar disk was higher than in the solar nebula. If we assume that the planets formed via the core accretion mechanism, as described, for example, by Hubickyj, Bodenheimer, & Lissauer (2005) we estimate that they contain at least 150 $M_{\rm Earth}$ of heavy elements. Here we include the high metallicity of the host star, 55 Cnc, with its [Fe/H]=+0.3 as representative of the planet's interior. Reconstituting this mass of solids to recover 55 Cancri's metallicity implies an original protostellar disk mass of $\sim 0.025 M_\odot$ within 6 AU. Assuming that the nascent disk extended to 30 AU with a $r^{-3/2}$ surface density profile, the total mass would have been

$\sim 0.06 M_\odot$, and the surface mass density in solids at 5 AU would have been 7 g cm$^{-2}$.

Adopting the reported orbital inclination of 53 deg for the outer planet McArthur et al. (2004) and assuming the orbits to be co-planar augments all masses by $1/\sin i = 1.25$. The resulting simplistic minimum mass protoplanetary nebula has 510 g cm$^{-2}$ for the average surface mass density of the combined gas and dust within 6 AU. Adopting a nominal gas to dust ratio of 100 yields a dust surface mass density of 5 g cm$^{-2}$.

But again considering the likely enrichment of solids within giant planets, and the associated H and He, yields an original mass within 6 AU of at least 0.031 M$_\odot$. Extending this disk to 30 AU gives a total mass of 0.075 M$_\odot$. The estimated surface mass density of solids in the disk at 5 AU would have been 8.7 g cm$^{-2}$.

For expected equilibrium disk temperatures, this minimum mass disk is below the threshold required for the development of non-axisymmetric gravitational instabilities (Laughlin & Rozyczka 1996), but likely high enough to support the formation of planets via core accretion (Robinson et al. 2006). In the context of this disk-profile scenario, the core accretion theory suggests that additional objects with masses ranging from Neptune to Saturn mass should be present beyond the frontier marked by the orbit of planet d, i.e. beyond 6 AU. If the outer planet migrated during or after its formation, the estimated disk properties computed here would be affected.

## 9. Discussion

Our eighteen year campaign of Doppler measurements of 55 Cnc at the Lick and Keck Observatories has gradually revealed additional superimposed wobbles, each best interpreted as due to another orbiting planet. The previously identified four planets revealed a large gap between 0.24 and 5.8 AU raising questions about unseen planets there and the planet formation history in the protoplanetary disk. The velocities presented here reveal a fifth periodicity with $P = 260$ d, consistent with Keplerian motion for which the most reasonable interpretation is another orbiting planet. The five-planet model suggests the new planet has a minimum mass of 45 M$_{\rm Earth}$ in a nearly circular orbit with a semimajor axis of $a = 0.781$AU. Thus, 55 Cnc is the first quintuple-planet system known.

This fifth planet apparently resides in the previously identified gap between 0.24-5.8 AU, and it remains between 0.73 AU (periastron) and 0.84 AU (apastron), preventing orbit crossings with both the next inner planet, "c", whose apastron is at 0.26 AU and the outer planet, "d", whose periastron is at 5.5 AU, ensuring dynamical stability that is demonstrated numerically by N-body simulations. As the star's luminosity is $L = 0.60$ L$_\odot$ (from its effective

temperature and radius), this fifth planet resides within the classical habitable zone. With a minimum mass of 45 $M_{Earth}$, we speculate that it contains a substantial amount of hydrogen and helium, not unlike Saturn ($M = 95$ $M_{Earth}$) in the solar system.

The four previously published planets around 55 Cancri now have revised orbital parameters and masses because the fifth planet had been contaminating the Doppler signal but was not taken into account. The orbital semimajor axes and masses of all five planets (moving outward from the central star) are $a = 0.038$ AU and $M \sin i = 10.8$ $M_{Earth}$; 0.115 AU and 0.824 $M_{Jup}$; 0.24 AU and 0.169 $M_{Jup}$; 0.781 AU and 0.144 $M_{Jup}$; and 5.77 AU and 3.83 $M_{Jup}$. All quoted minimum masses are uncertain by $\sim$5% due to the uncertain mass of the host star 55 Cnc. The planets in this system all have nearly circular orbits, with the caveat that the orbital eccentricity for the 260 d planet is poorly constrained by radial velocity data.

The inclination of the orbital plane of the outer planet has been estimated from the apparent astrometric motion of the star, as measured with the Fine Guidance Sensor of the Hubble Space Telescope (McArthur et al. 2004). The derived orbital inclination is $i = 53\pm6.8$ deg (37 deg from edge-on) for that outer planet, implying that its actual mass is 4.9 $M_{Jup}$. Assuming coplanarity for the other four planets, their actual masses (proceeding outward) are $M_e = 13.5$ $M_{Earth}$ (nearly one Uranus mass), $M_b = 1.03$ $M_{Jup}$, $M_c = 0.21$ $M_{Jup} = 66.7$ $M_{Earth}$, and $M_f = 0.18$ $M_{Jup} = 57$ $M_{Earth}$. Normally, co-planarity should not be a foregone conclusion, as the eccentricities of many exoplanets imply a dynamically perturbative history. But for the 55 Cnc system with its five planets so vulnerable to instabilities, such an active past seems unlikely. Any great perturbations would have ejected the smaller planets. Thus the planetary orbits in 55 Cnc are likely to reside in a flattened plane, analogous to the ecliptic, coinciding with the original protoplanetary disk out of which the planets presumably formed.

If 55 Cnc did have a quiescent past, the star's spin axis should be nearly coincident with the normal of the system's orbital plane. The inclination of the spin axis can be determined from the spectroscopically measured rotational $v \sin i = 2.46$ km s$^{-1}$ and the photometrically determined spin period of 42.7 d for the star, along with its radius of 0.93 R$_\odot$. The 42.7 d spin period implies an equatorial velocity of only 1.24 km s$^{-1}$, which is lower than $v \sin i$, an impossibility. Either the measured $v \sin i$ is too high by a factor of two (quite possible given the many line broadening sources) or the spin period is much shorter (not likely, given the low chromospheric activity). As is common, the inclination of the spin axis of a nearby star, as attempted here, carries uncertainties so large as to be of little value. Nonetheless the crude interpretation would be that the star is not viewed pole-on. Indeed, if the orbits were viewed nearly pole-on the implied planetary masses would be so large as to render the

system dynamically unstable. We conclude that the orbital plane of 55 Cnc is not being viewed nearly pole-on, consistent with the astrometric value of $i$=53 deg.

As the 55 Cnc system has more planets than any previously discovered system, its overall structure, including its planet mass distribution, its density of orbits, and its orbital eccentricities, offers direct constraints about its protoplanetary disk and subsequent planetary dynamics. The 55 Cnc system may initially be sketched as having one massive planet, likely a hydrogen-helium gas giant, in a nearly circular orbit at 5.8 AU. Inward are four less massive planets, the innermost being roughly Uranus mass, the next outward having roughly Jupiter mass and likely gaseous, and the next two having somewhat sub-Saturn masses, also probably gaseous. The outer planet has an orbital angular momentum quickly shown to be at least $8.2 \times 10^{43}$ kg m$^2$ s$^{-1}$, certainly 100 times greater than the star's $spin$ angular momentum, $6.1 \times 10^{41}$ kg m$^2$ s$^{-1}$ (from its 42.7 d spin period).

Thus, 55 Cnc contains a dominant outer planet at 5.8 AU of roughly 5 M$_{Jup}$ and four lower mass planets, all five in nearly circular orbits (though two orbits appear to be somewhat more eccentric than found for the more massive planets in our solar system). The large eccentricities found in the majority of exoplanets (Marcy et al. 2005; Butler et al. 2006) are not seen in 55 Cnc. The five orbits in 55 Cnc are probably nearly co-planar, as discussed above, lest some planet masses be too large to allow stability. Thus, 55 Cnc system has some basic structural attributes found in our solar system: nearly coplanar, circular orbits, with a dominant gas giant between 5-6 AU. This similarity suggests that such solar system architectures are not extremely rare.

The formation of multi-planet systems with outer, dominant planets may occasionally form such that they persist for billions of years without disruptive gravitational perturbations that cause large eccentricities and eject planets. Because nested, coplanar, circular orbits could hardly be obtained unless they began that way, the 55 Cnc system, along with the solar system, supports the hypothesis that planets form in viscous protoplanetary disks, as has long been predicted by standard planet formation theory, e.g., Lissauer (1995).

One puzzle is whether the 55 Cnc planets suffered significant migration. The 44.35 d and 14.65 d have a period ratio of 3.027:1.000, thus leaving open the possibility of a mean motion resonance identified previously (Marcy et al. 2002). As planets have no reason to form with integer period ratios, any resonance suggests that some differential migration occurred, allowing the two planets to capture each other. However the 3:1 mean motion resonance was found to be absent in the current N-body model as none of the relevant resonant arguments are librating.

However, if migration occurred, we wonder what prevented the outer planet, and indeed

all of the planets, from migrating inward. Perhaps the disk dissipated just as this last crop of five planets formed, as suggested in some migrational models (Lin et al. 2000; Trilling, Lunine, & Benz 2002; Armitage et al. 2002; Armitage, Clarke, & Palla 2003; Ida & Lin 2004, 2005; Narayan, Cumming, & Lin 2005). Indeed, the proximity of the three inner planets to the host star, especially the Jupiter-mass planet at 0.115 AU ($P = 14.65$ d), suggests that they migrated inward to their present locations, assuming they did not form in situ. If so, protoplanetary disk material likely orbited outside 0.24 AU, exerting an inward torque on those planets and carrying away orbital angular momentum in the system. During the migration period, the implied disk material would have had a mass comparable to (or exceeding) the Jovian-mass planets, from which the most recently identified planet at 0.78 AU could have formed.

It is interesting that the third and fourth planets (at 0.24 and 0.78 AU) have small minimum masses, under 0.2 $M_{Jup}$, but are surrounded by much larger giant planets with minimum masses of 0.824 and 3.8 $M_{Jup}$. One wonders why the acquisition of material was apparently so different among these four planets.

One also wonders why this particular star ended up with five planets while 90 percent of stars on Doppler surveys do not have any detected giant planets. A statistical analysis of the planet detectability and observational incompleteness has been carried out by Cumming et al. 2007. Perhaps the high metallicity of 55 Cnc ([Fe/H] $= +0.30$) played a role in the efficient planet formation. Fischer & Valenti (2005) find a correlation not only between stellar metallicity and the occurrence of planets, but also between high metallicity and multi-planet systems. But we doubt that a mere factor of two enhancement in heavy elements could account entirely for the five planets in this system. Some stochasticity in planet formation and subsequent stability must play a role.

The outer planet at 5.8 AU is angularly separated from the star ($d = 12.5$ pc) by 0.47 arcseconds making it a good target for next-generation adaptive optics systems. The Space Interferometry Mission, "SIM PlanetQuest", operating in narrow angle mode with astrometric precision of 1 $\mu$as could measure the astrometric wobble caused by all four outer planets, providing definitive masses and orbital inclinations for them. A spaceborn coronagraph or a spaceborn interferometer might be capable of imaging the outer planet and taking spectra of it. NASA and ESA have a wonderful opportunity to fund such an imaging telescope, thereby detecting and spectroscopically assessing a mature extrasolar planet. Moreover, as 55 Cancri is metal-rich, the planets may also be abundant in heavy elements, offering an opportunity to study rich atmospheric chemistry, clouds, and weather, if spectra could be obtained. Transits, if any occur, would provide planet radii offering information about potential rocky cores.

This rich planetary system portends a fruitful future for the Doppler technique of studying exoplanets. It shows that extending the time baseline of Doppler measurements can reveal multiple planets, the existence or absence of which provides information about the formation, structure, and evolution of planetary systems.

# REFERENCES

Adams, F. C., & Laughlin, G. 2006, ApJ, 649, 1004–1009

Armitage, P. J., Livio, M., Lubow, S. H., & Pringle, J. E. 2002, MNRAS, 334, 248–256

Armitage, P. J., Clarke, C. J., & Palla, F. 2003, MNRAS, 342, 1139–1146

Baliunas, S. L., Donahue, R. A., Soon, W., & Henry, G. W. 1998, In Cool Stars, Stellar Systems, and the Sun, R. A. Donahue and J. A. Bookbinder, eds., volume 154 of *Astronomical Society of the Pacific Conference Series*, pp. 153–+

Bodenheimer, P., Laughlin, G., & Lin, D. N. C. 2003, ApJ, 592, 555–563

Boss, A. P. 1997, Science, 276, 1836–1839

Bryden, G., Beichman, C. A., Trilling, D. E., Rieke, G. H., Holmes, E. K., Lawler, S. M., Stapelfeldt, K. R., Werner, M. W., Gautier, T. N., Blaylock, M., Gordon, K. D., Stansberry, J. A., & Su, K. Y. L. 2006, ApJ, 636, 1098–1113

Butler, R. P., Marcy, G. W., Williams, E., McCarthy, C., Dosanjh, P., & Vogt, S. S. 1996, PASP, 108, 500

Butler, R. P., Marcy, G. W., Williams, E., Hauser, H., & Shirts, P. 1997, ApJ, 474, L115+

Butler, R. P., Marcy, G. W., Fischer, D. A., Brown, T. M., Contos, A. R., Korzennik, S. G., Nisenson, P., & Noyes, R. W. 1999, ApJ, 526, 916–927

Butler, R. P., Vogt, S. S., Marcy, G. W., Fischer, D. A., Wright, J. T., Henry, G. W., Laughlin, G., & Lissauer, J. J. 2004, ApJ, 617, 580–588

Butler, R. P., Wright, J. T., Marcy, G. W., Fischer, D. A., Vogt, S. S., Tinney, C. G., Jones, H. R. A., Carter, B. D., Johnson, J. A., McCarthy, C., & Penny, A. J. 2006, ApJ, 646, 505–522

Eggenberger, A., Udry, S., & Mayor, M. 2004, A&A, 417, 353–360

ESA, . 1997, VizieR Online Data Catalog, 1239, 0–+

Fischer, D. A. & Valenti, J. A. 2005, ApJ, 632, 1102–1117

Froehlich, C., Anklin, M., Crommelynck, D., Finsterle, W., & Willson, R. C. 1998, In New Eyes to See Inside the Sun and Stars, F.-L. Deubner, J. Christensen-Dalsgaard, and D. Kurtz, eds., volume 185 of *IAU Symposium*, pp. 89–+

Grillmair, C. J., Charbonneau, D., Burrows, A., Armus, L., Stauffer, J., Meadows, V., Van Cleve, J., & Levine, D. 2007, ApJ, 658, L115–L118

Hall, J. C., Henry, G. W., & Lockwood, G. W. 2007, AJ, 133, 2206–2208

Henry, G. W. 1999, PASP, 111, 845–860

Henry, G. W., Baliunas, S. L., Donahue, R. A., Fekel, F. C., & Soon, W. 2000, ApJ, 531, 415–437

Hubickyj, O., Bodenheimer, P., & Lissauer, J. J. 2005, Icarus, 179, 415–431

Ida, S., & Lin, D. N. C. 2004, ApJ, 604, 388–413

Ida, S., & Lin, D. N. C. 2005, ApJ, 626, 1045–1060

Kjeldsen, H., et al. 2005, ApJ, 635, 1281

Laughlin, G., & Rozyczka, M. 1996, ApJ, 456, 279–+

Lin, D. N. C., Papaloizou, J. C. B., Terquem, C., Bryden, G., & Ida, S. 2000, Protostars and Planets IV, pp. 1111–+

Lissauer, J. J. 1995, Icarus, 114, 217–236

Maness, H. L., Marcy, G. W., Ford, E. B., Hauschildt, P. H., Shreve, A. T., Basri, G. B., Butler, R. P., & Vogt, S. S. 2007, PASP, 119, 90–101

Marcy, G., Butler, R. P., Fischer, D., Vogt, S., Wright, J. T., Tinney, C. G., & Jones, H. R. A. 2005, Progress of Theoretical Physics Supplement, 158, 24–42

Marcy, G. W., Butler, R. P., Fischer, D. A., Laughlin, G., Vogt, S. S., Henry, G. W., & Pourbaix, D. 2002, ApJ, 581, 1375–1388

McArthur, B. E., Endl, M., Cochran, W. D., Benedict, G. F., Fischer, D. A., Marcy, G. W., Butler, R. P., Naef, D., Mayor, M., Queloz, D., Udry, S., & Harrison, T. E. 2004, ApJ, 614, L81–L84

Murray, C. D., & Dermott, S. F. 1999. Solar system dynamics, Solar system dynamics by Murray, C. D., 1999 (Cambridge: Cambridge University Press)

Narayan, R., Cumming, A., & Lin, D. N. C. 2005, ApJ, 620, 1002–1009

Noyes, R. W., Hartmann, L. W., Baliunas, S. L., Duncan, D. K., & Vaughan, A. H. 1984, ApJ, 279, 763–777

Paulson, D. B., Saar, S. H., Cochran, W. D., & Henry, G. W. 2004, AJ, 127, 1644–1652

Press, W. H., Teukolsky, S. A., Vetterling, W. T., & Flannery, B. P. 1992. Numerical recipes in FORTRAN. The art of scientific computing, Cambridge: University Press, —c1992, 2nd ed.

Queloz, D., Henry, G. W., Sivan, J. P., Baliunas, S. L., Beuzit, J. L., Donahue, R. A., Mayor, M., Naef, D., Perrier, C., & Udry, S. 2001, A&A, 379, 279–287

Raghavan, D., Henry, T. J., Mason, B. D., Subasavage, J. P., Jao, W.-C., Beaulieu, T. D., & Hambly, N. C. 2006, ApJ, 646, 523–542

Raymond, S. N., Barnes, R., & Kaib, N. A. 2006, ApJ, 644, 1223–1231

Richardson, L. J., Deming, D., Horning, K., Seager, S., & Harrington, J. 2007, Nature, 445, 892–895

Rivera, E. J., Lissauer, J. J., Butler, R. P., Marcy, G. W., Vogt, S. S., Fischer, D. A., Brown, T. M., Laughlin, G., & Henry, G. W. 2005, ApJ, 634, 625–640

Robinson, S. E., Laughlin, G., Bodenheimer, P., & Fischer, D. 2006, ApJ, 643, 484–500

Santos, N. C., Bouchy, F., Mayor, M., Pepe, F., Queloz, D., Udry, S., Lovis, C., Bazot, M., Benz, W., Bertaux, J.-L., Lo Curto, G., Delfosse, X., Mordasini, C., Naef, D., Sivan, J.-P., & Vauclair, S. 2004, A&A, 426, L19–L23

Sato, B., Fischer, D. A., Henry, G. W., Laughlin, G., Butler, R. P., Marcy, G. W., Vogt, S. S., Bodenheimer, P., Ida, S., Toyota, E., Wolf, A., Valenti, J. A., Boyd, L. J., Johnson, J. A., Wright, J. T., Ammons, M., Robinson, S., Strader, J., McCarthy, C., Tah, K. L., & Minniti, D. 2005, ApJ, 633, 465–473

Schneider, G., Becklin, E. E., Smith, B. A., Weinberger, A. J., Silverstone, M., & Hines, D. C. 2001, AJ, 121, 525–537

Seagroves, S., Harker, J., Laughlin, G., Lacy, J., & Castellano, T. 2003, PASP, 115, 1355–1362

Takeda, G., Ford, E. B., Sills, A., Rasio, F. A., Fischer, D. A., & Valenti, J. A. 2007, ApJS, 168, 297–318

Trilling, D. E., Lunine, J. I., & Benz, W. 2002, A&A, 394, 241–251

Valenti, J. A., & Fischer, D. A. 2005, ApJS, 159, 141–166

VandenBerg, D. A., & Clem, J. L. 2003, AJ, 126, 778–802

Vaníček, P. 1971, Ap&SS, 12, 10–+

Vogt, S. S. 1987, PASP, 99, 1214–1228

Vogt, S. S., Allen, S. L., Bigelow, B. C., Bresee, L., Brown, B., Cantrall, T., Conrad, A., Couture, M., Delaney, C., Epps, H. W., Hilyard, D., Hilyard, D. F., Horn, E., Jern, N., Kanto, D., Keane, M. J., Kibrick, R. I., Lewis, J. W., Osborne, J., Pardeilhan, G. H., Pfister, T., Ricketts, T., Robinson, L. B., Stover, R. J., Tucker, D., Ward, J., & Wei, M. Z. 1994, In Proc. SPIE Instrumentation in Astronomy VIII, David L. Crawford; Eric R. Craine; Eds., Volume 2198, p. 362, pp. 362–+

Willson, R. C. 1977, Science, 277, 1963

Wisdom, J. 2005. "A Neptune-sized Planet in the rho 1 Cancri System." DDA meeting 36, 05.08; Bulletin of the American Astronomical Society, Vol. 37, 525

Wright, J. T. 2005, PASP, 117, 657–664

Wright, J. T., Marcy, G. W., Butler, R. P., & Vogt, S. S. 2004, ApJS, 152, 261–295

Yi, S. K., Demarque, P., & Kim, Y.-C. 2004, Ap&SS, 291, 261–262

Table 1.   Velocities for 55 Cancri: Lick & Keck

| JD<br>-2440000 | Vel.<br>$(m\ s^{-1})$ | Unc.<br>$(m\ s^{-1})$ | Tele. |
|---|---|---|---|
| 7578.730 | 25.67 | 9.7 | L |
| 7847.044 | 3.91 | 8.4 | L |
| 8017.688 | 31.45 | 7.5 | L |
| 8375.669 | -31.38 | 8.8 | L |

Note. — Table 1 is presented in its entirety in the electronic edition of the Astrophysical Journal. A portion is shown here for guidance regarding its form and content.

Table 2.    Orbital Parameters for the Five-Planet Model

| Star | Period (days) | $T_p$ | $e$ | $\omega$ (deg) | $K$ (m s$^{-1}$) | M sin $i$ (M$_{Jup}$) | $a$ (AU) |
|---|---|---|---|---|---|---|---|
| [1]Planet e | 2.81705 | 2449999.83643 | 0.07 | 248.9 | 5.07 | 0.034 | 0.038 |
| ± | 0.0001 | 0.0001 | 0.06 | 38 | 0.53 | 0.0036 | 1.0×10$^{-6}$ |
| Planet b | 14.65162 | 2450002.94749 | 0.014 | 131.94 | 71.32 | 0.824 | 0.115 |
| ± | 0.0007 | 1.2 | 0.008 | 30 | 0.41 | 0.007 | 1.1×10$^{-6}$ |
| Planet c | 44.3446 | 2449989.3385 | 0.086 | 77.9 | 10.18 | 0.169 | 0.240 |
| ± | 0.007 | 3.3 | 0.052 | 29 | 0.43 | 0.008 | 4.5×10$^{-5}$ |
| Planet f | 260.00 | 2450080.9108 | 0.2(f) | 181.1 | 4.879 | 0.144 | 0.781 |
| ± | 1.1 | 1.1 | 0.2 | 60. | 0.6 | 0.04 | 0.007 |
| Planet d | 5218 | 2452500.6 | 0.025 | 181.3 | 46.85 | 3.835 | 5.77 |
| ± | 230 | 230 | 0.03 | 32 | 1.8 | 0.08 | 0.11 |

[1]Planets are listed in order of increasing orbital period, however the planet designations, b-f, correspond to the chronological order of their discovery.

[f]ecc. fixed

Table 3.   Summary of improvments in RMS and $\chi^2_\nu$ fits

| Planet | RMS [m s$^{-1}$] | $\sqrt{\chi^2_\nu}$ |
|--------|------------------|---------------------|
| b,c | 11.28 | 3.42 |
| b,c,d | 8.62 | 2.50 |
| b,c,d,e | 7.87 | 2.12 |
| b,c,d,e,f | 6.74 | 1.67 |

Table 4. Orbital Parameters from Self-Consistent Dynamical fit

| Planet | Period (days) | $T_p$ (JD-2440000) | $e$ | $\omega$ (deg) | $K$ (m s$^{-1}$) | M$\sin i$ (M$_{Jup}$) | $a$ (AU) |
|---|---|---|---|---|---|---|---|
| 55 Cancri b [a] | 14.651262 | 7572.0307 | 0.0159 | 164.001 | 71.84 | 0.8358 | 0.115 |
| 55 Cancri c | 44.378710 | 7547.5250 | 0.0530 | 57.405 | 10.06 | 0.1691 | 0.241 |
| 55 Cancri d | 5371.8207 | 6862.3081 | 0.0633 | 162.658 | 47.20 | 3.9231 | 5.901 |
| 55 Cancri e | 2.796744 | 7578.2159 | 0.2637 | 156.500 | 3.73 | 0.0241 | 0.038 |
| 55 Cancri f | 260.6694 | 7488.0149 | 0.0002 | 205.566 | 4.75 | 0.1444 | 0.785 |

[a]Epoch= JD 2447578.730, $\sqrt{\chi^2} = 2.012$ (without jitter included), RMS=7.71 ms$^{-1}$.

Table 5.   Results of Photometric Transit Search

| Planet | Planetary Period (days) | Semi-Amplitude (mag) | Transit Probability (%) | Predicted Transit Depth (mag) | Observed Transit Depth (mag) | Transits |
|---|---|---|---|---|---|---|
| e | 2.79565 | 0.00004 ± 0.00006 | 9.7 | +0.00065 | +0.00029±0.00020 | No? |
| b | 14.65165 | 0.00006 ± 0.00006 | 4.1 | +0.0143 | +0.0007±0.0005 | No |
| c | 44.3401 | 0.00008 ± 0.00006 | 2.0 | +0.0086 | −0.0003±0.0006 | No |
| f | 260.81 | 0.00008 ± 0.00006 | 0.8 | +0.0090 | ... [a] | No: |
| d | 5223 | ... [b] | 0.1 | +0.0155 | ... [c] | ? |

[a]No observations in predicted 12-hr transit window but many observations within the one sigma uncertainty interval.

[b]Duration of the photometric record is less than the planetary orbital period.

[c]Poorly constrained orbit and insufficient photometric phase coverage.
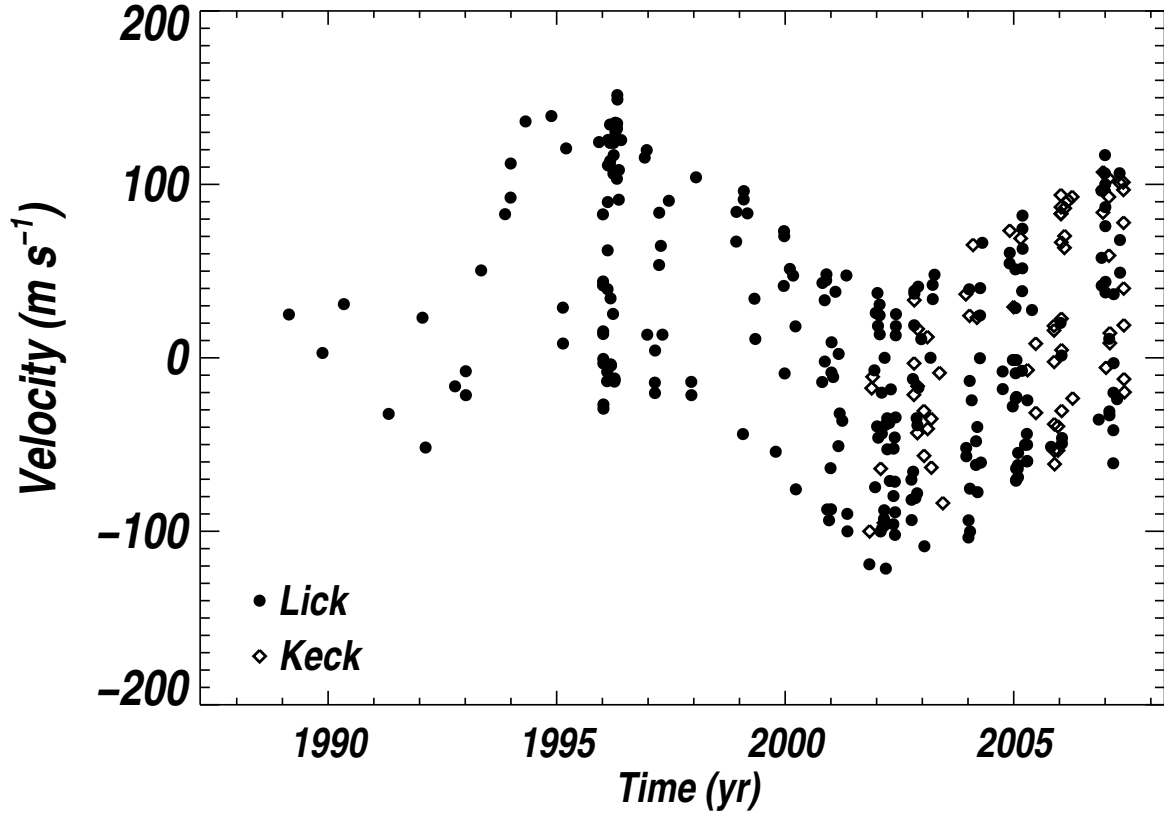
Fig. 1.— Measured velocities for 55 Cancri from Lick and Keck obtained from 1989.1 to 2007.4. Data from Lick (filled dots) had errors of $\sim$10 m s$^{-1}$ prior to 1994 and 3–5 m s$^{-1}$ thereafter. Data from Keck (open diamonds) had errors of $\sim$3 m s$^{-1}$ prior to 2004 August, and 1.0–1.5 m s$^{-1}$ thereafter. The 14-year period from the outer planet and the short timescale variations from the 14.6-day planet are apparent to the eye.
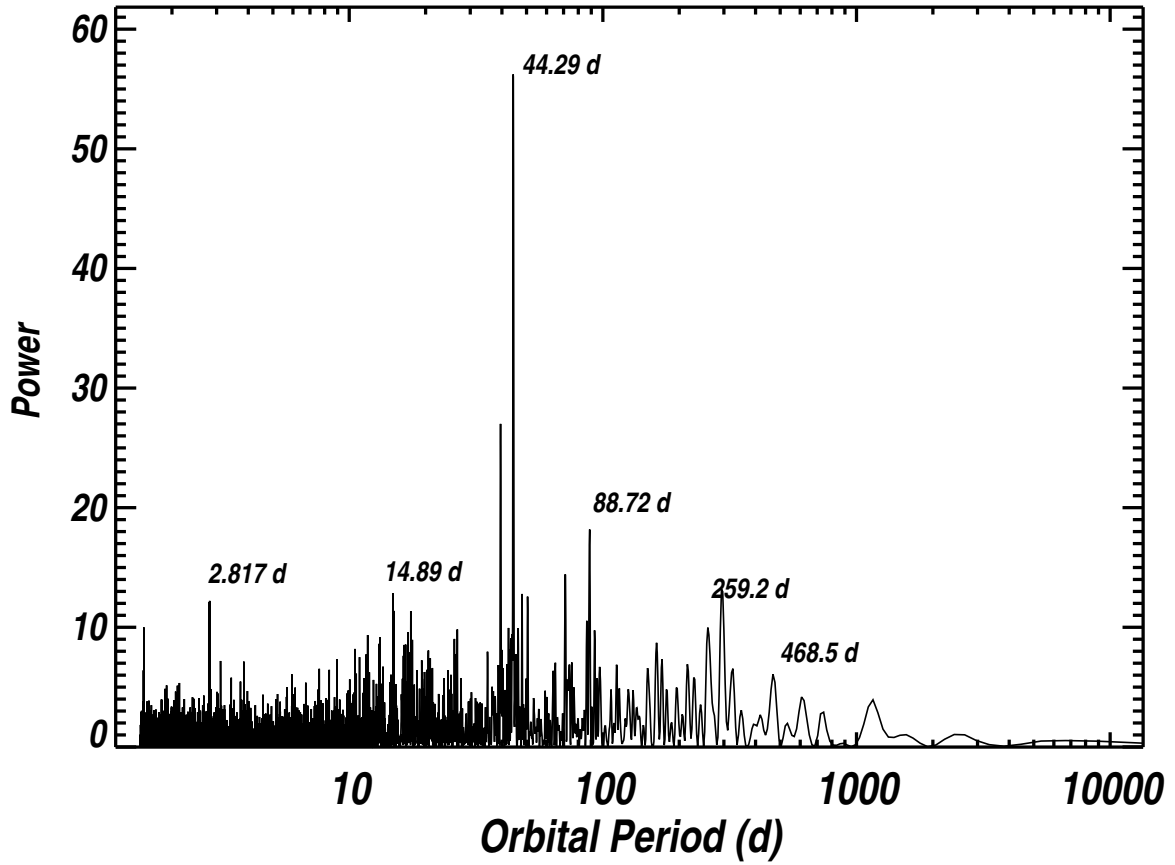
Fig. 2.— Periodogram of the residuals to a Keplerian model that contains only the two well established planets with periods of 14.65 d and 5200 d. The tall peak at P = 44.3 d confirms the previously suspected planet with that period.
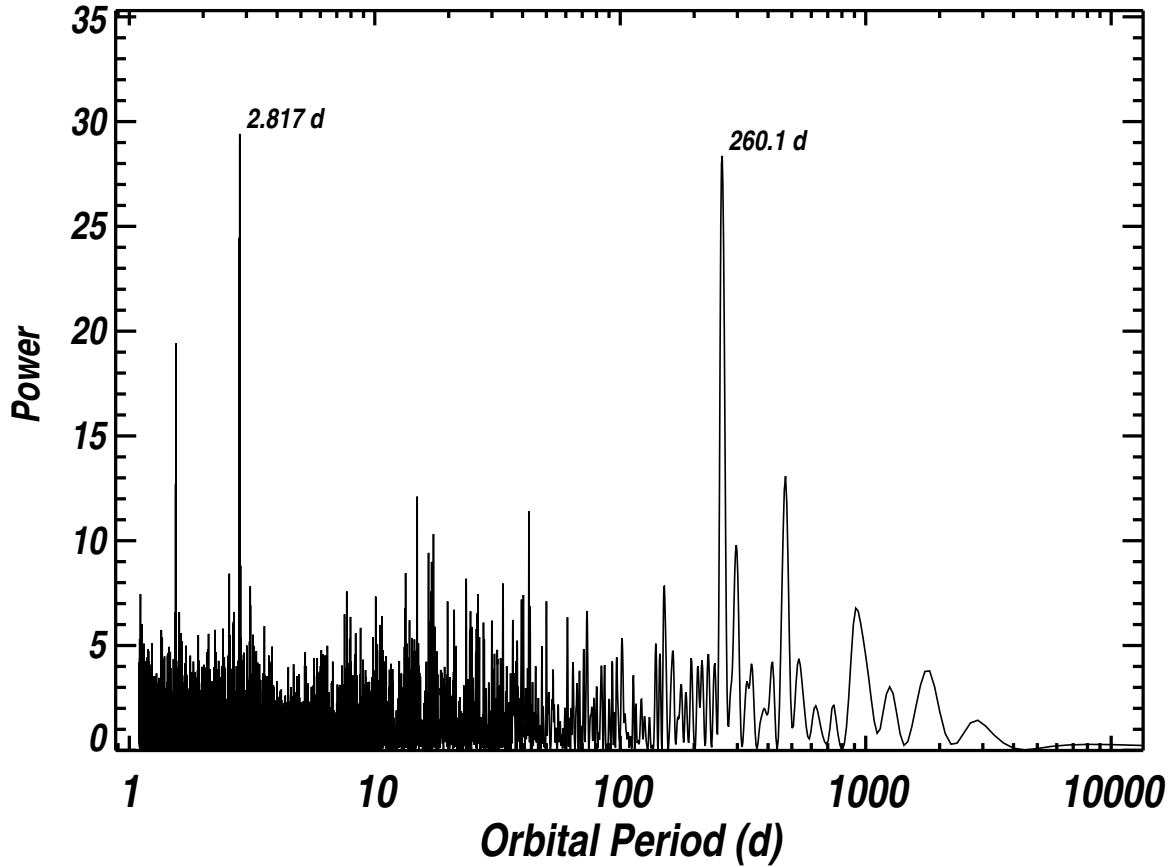
Fig. 3.— Periodogram of the residuals to a Keplerian model that contains three known planets with periods of 14.6 d, 44.3 d, and 5200 d. The tallest peaks are at 2.81 d and 260 d suggesting the existence of real periodicities in the velocities. The peak at ∼1.5 d is an alias of the 2.8 d peak, and the peak at 460 d is an alias of that at 260 d that disappears after modeling all five planets.
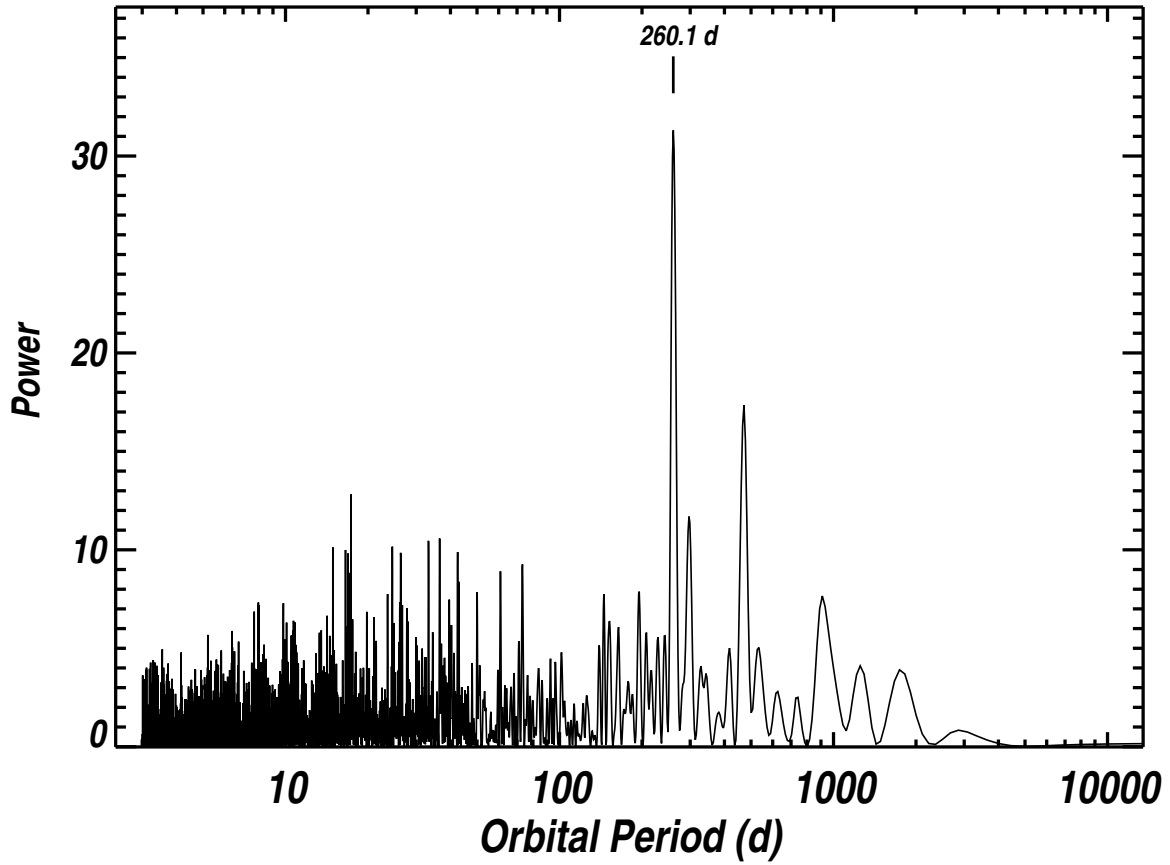
Fig. 4.— Periodogram of the residuals to a Keplerian model that contains the four previously suspected planets with periods near 2.817 d, 14.65 d, 44.3 d, and 5200 d. The periodogram exhibits a peak at 260.0 d, caused by the prospective fifth planet in the system. The smaller peak to its right at 460 d is an alias.
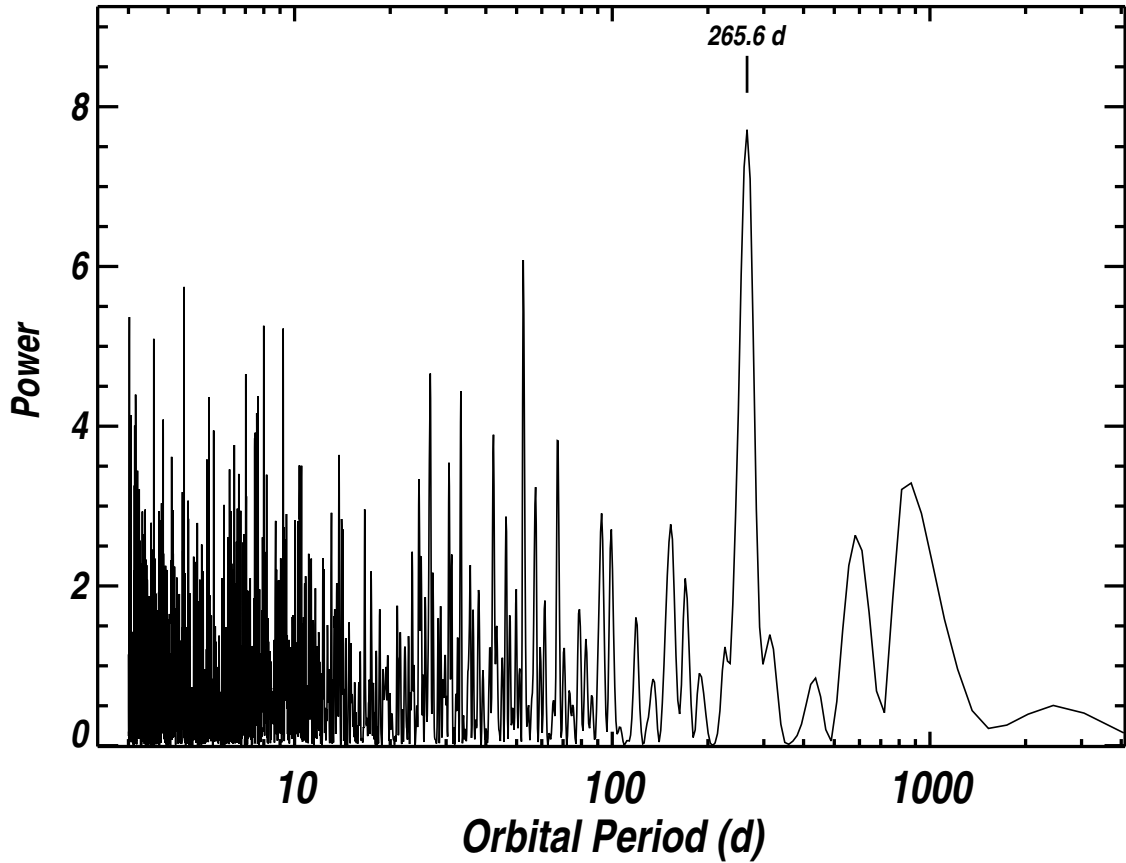
Fig. 5.— Periodogram of the residuals to a 4-planet Keplerian model, as in Figure 4, but fit to the Keck velocities only. The tallest peak is at a period of 265.6 d, nearly the same as that emerging from the Lick data. The modest peak power of only 7.7 is consistent with the limited time sampling and duration of the Keck observations. No other period is compelling between periods of 1 and 3000 d.
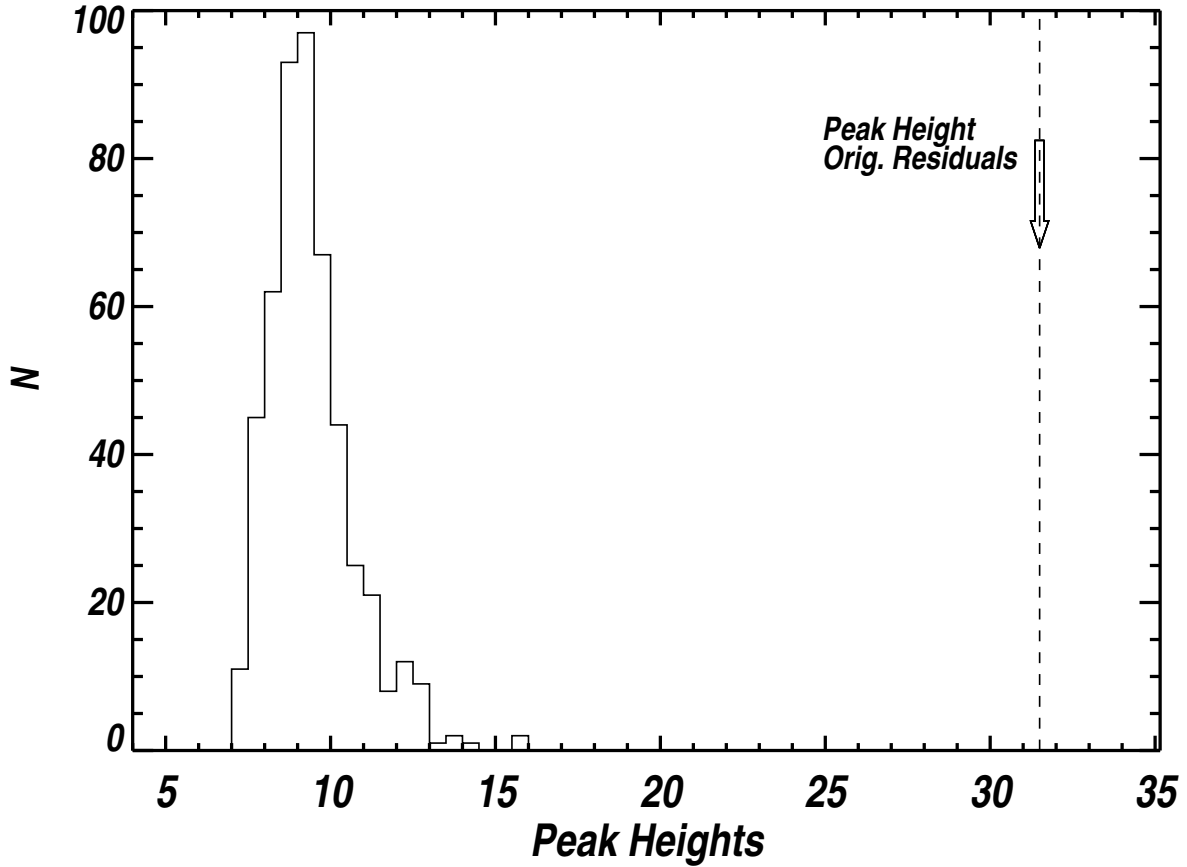
Fig. 6.— A test of the False Alarm Probability of the 260 d periodicity seen in the combined velocities from both Lick and Keck (Figure 4). The residuals to a 4-planet model were scrambled 500 times, yielding a histogram of the highest power in the periodograms. The power of 31.5 from the original residuals (Figure 4) is greater than that from all 500 trials, implying an FAP for the 260 d period of less than 0.002, suggesting that it is real.
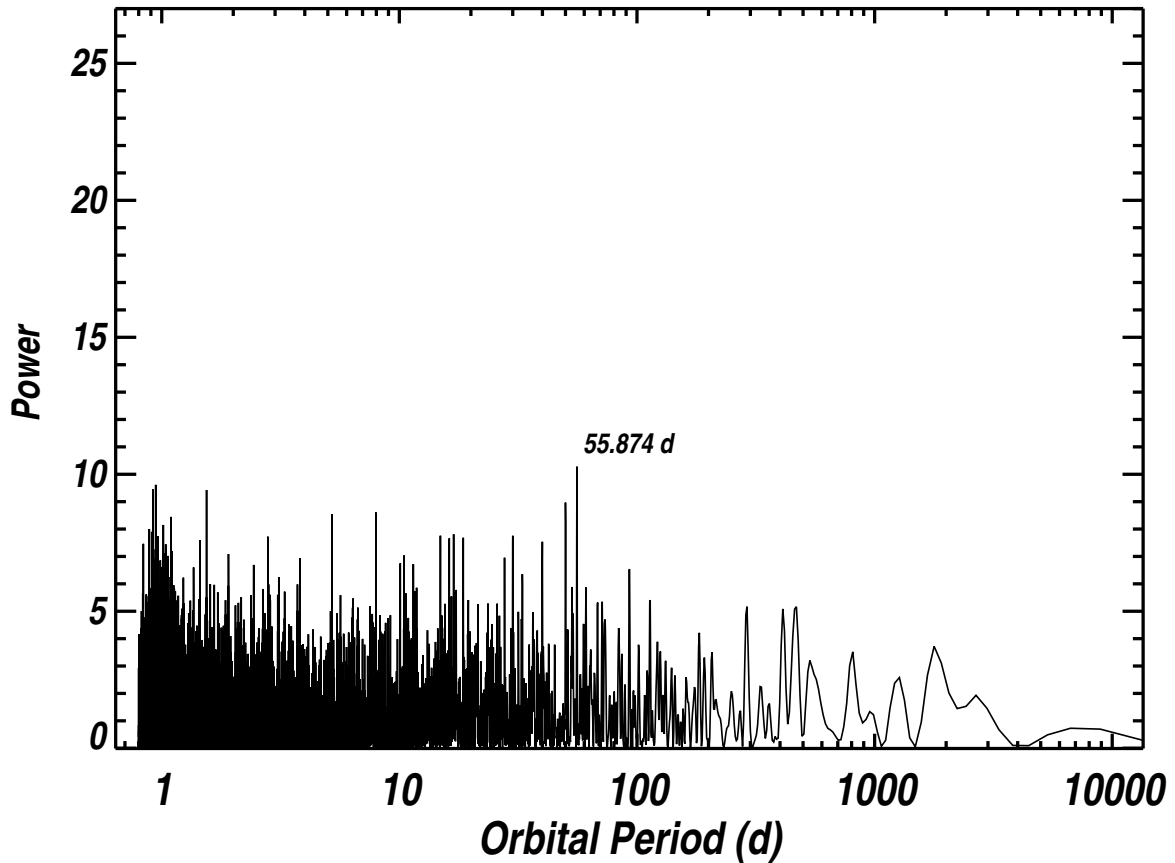
Fig. 7.— Periodogram of the velocity residuals to a Keplerian model that contains five planets including the prospective new planet at $P \approx 260$ d. Velocities from both Lick and Keck are included. The peak that had been apparent at 260 d in the residuals to a 4-planet model (Figures 4 and 5) has vanished due to its inclusion in the 5-planet model. No other compelling periods are apparent.
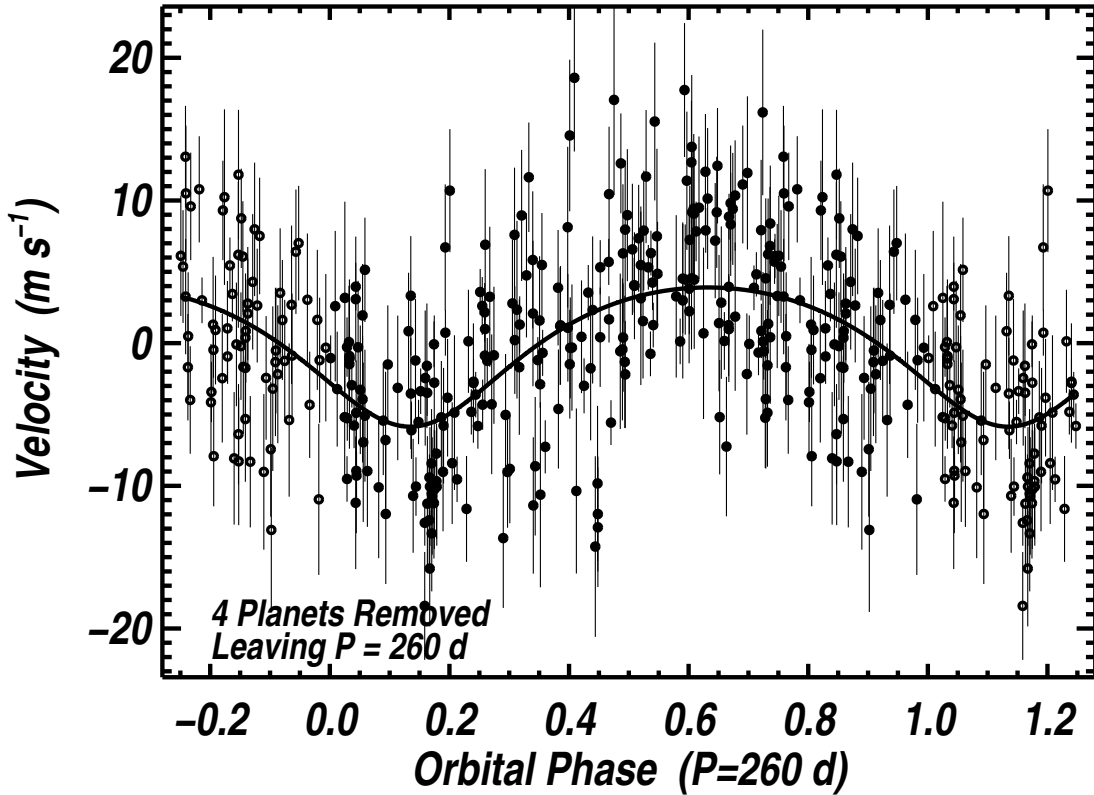
Fig. 8.— Residual velocities vs orbital phase (for P = 260 d) after the velocities induced by the four other planets are subtracted. The orbital parameters were established with a simultaneous 5-planet Keplerian fit to all Doppler measurements. The residual velocities reveal the periodic variation associated with the new planet. The solid line shows the Keplerian curve of the 260 d planet alone, with eccentricity frozen to 0.2. The planet's minimum mass is 45 $M_{Earth}$ and the semimajor axis is 0.78 AU.
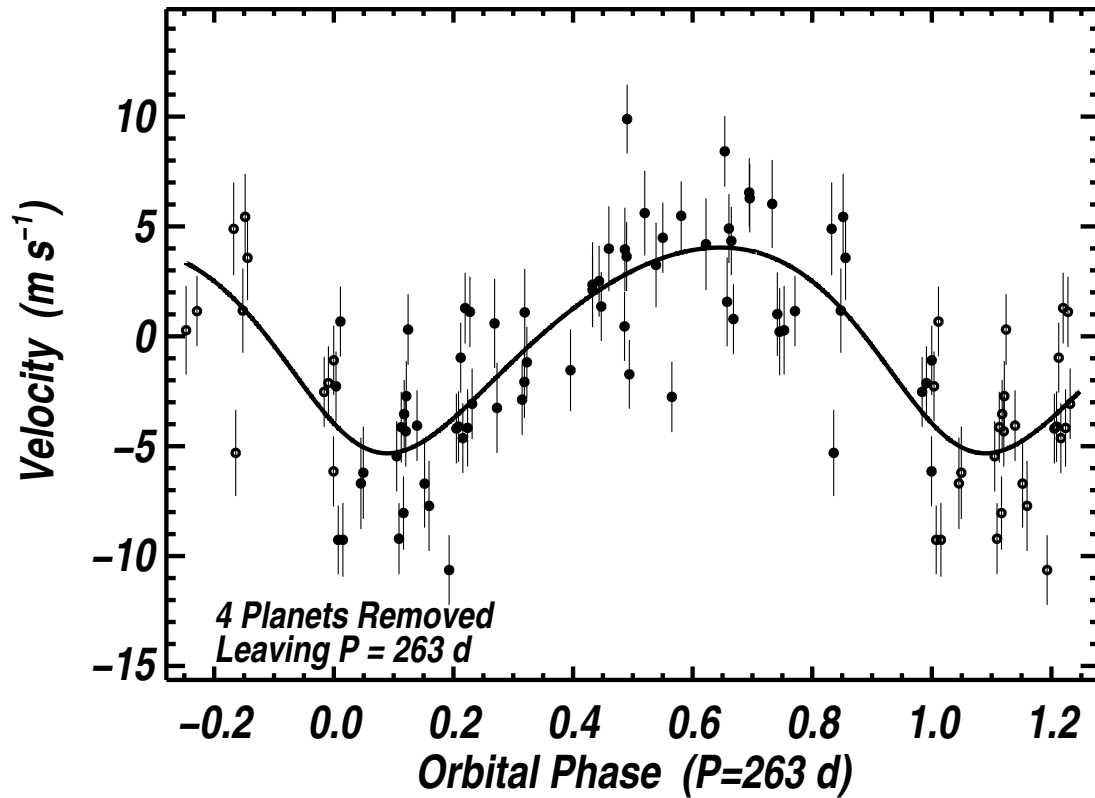
Fig. 9.— Velocity of the new planet vs. orbital phase, as with Figure 8, but for Keck velocities only. The periodicity near 260 d is apparent independently in the Keck velocities. The best-fit to the Keck velocities yields an eccentricity of $e$=0.16, only marginally significant.
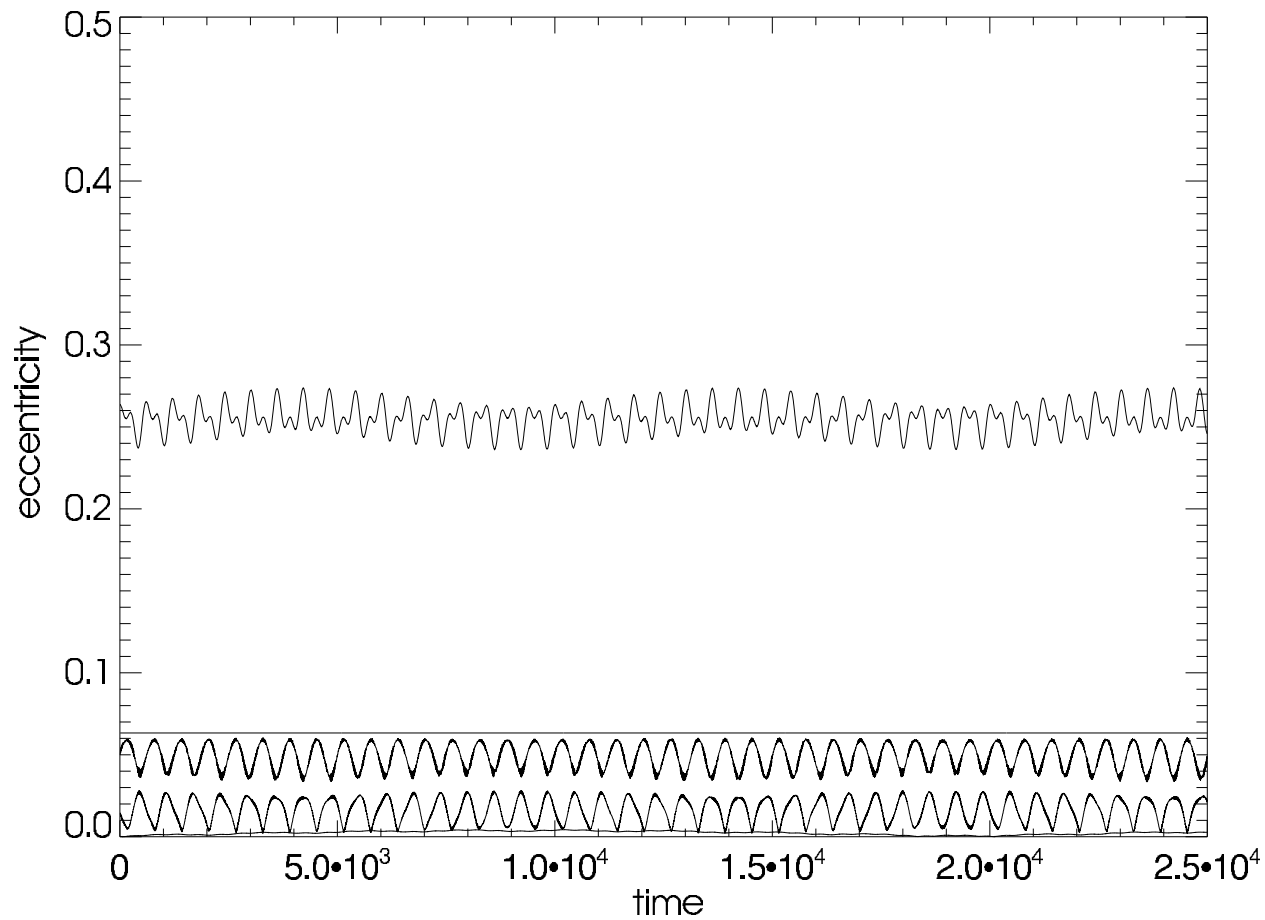
Fig. 10.— Eccentricity variations arising from an N-body numerical integration of the five-planet model listed in Table 2.
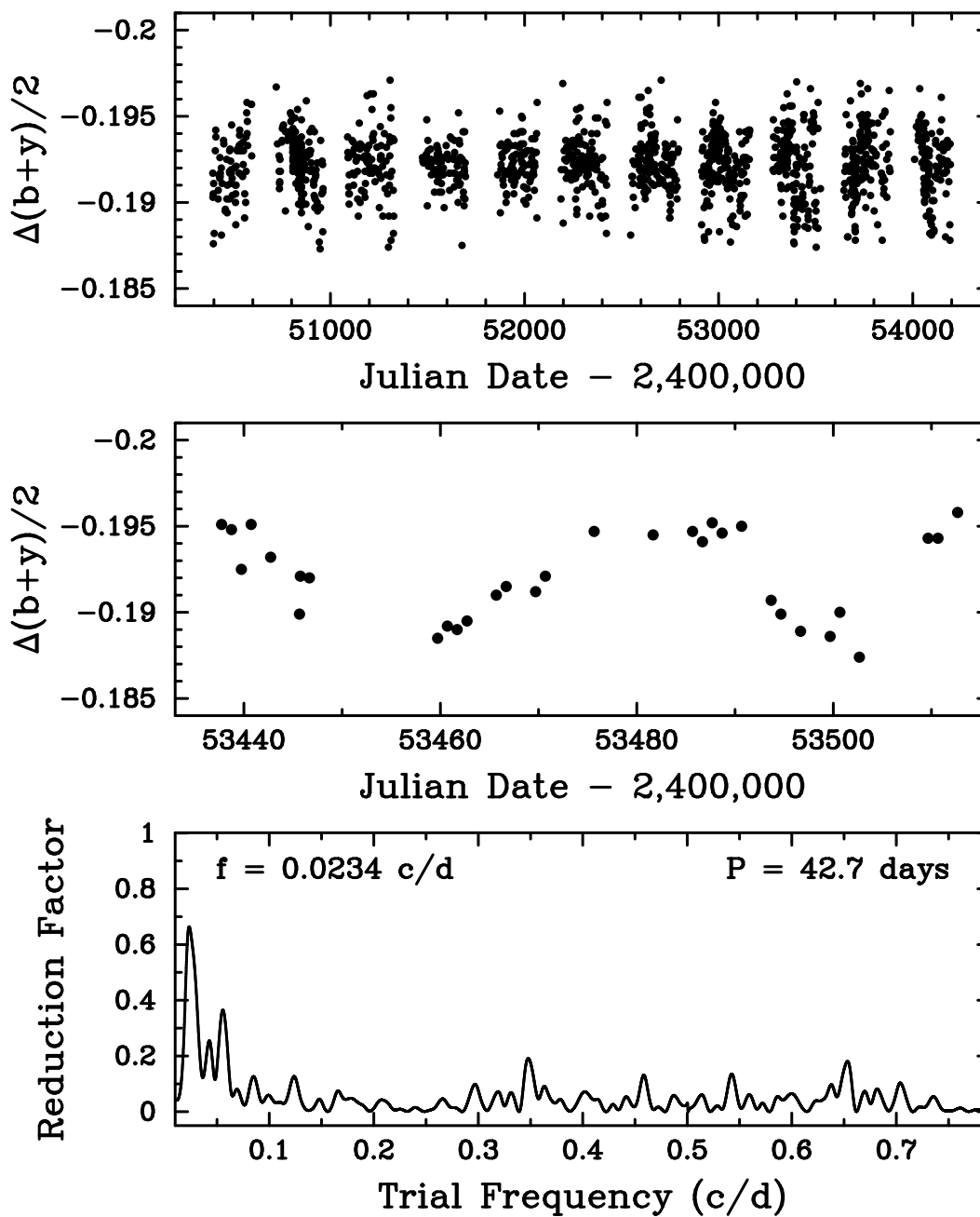
Fig. 11.— The 11-yr Strömgren photometric data set of 55 Cnc (*top panel*). The data have been normalized so that the annual means are identical. A portion of the ninth observing season (*middle panel*) shows coherent photometric variability in 55 Cnc due to rotational modulation in the visibility of starspots. The power spectrum of the data in the middle panel (*bottom panel*) reveals the star's rotation period of 42.7 ± 2.5 days.
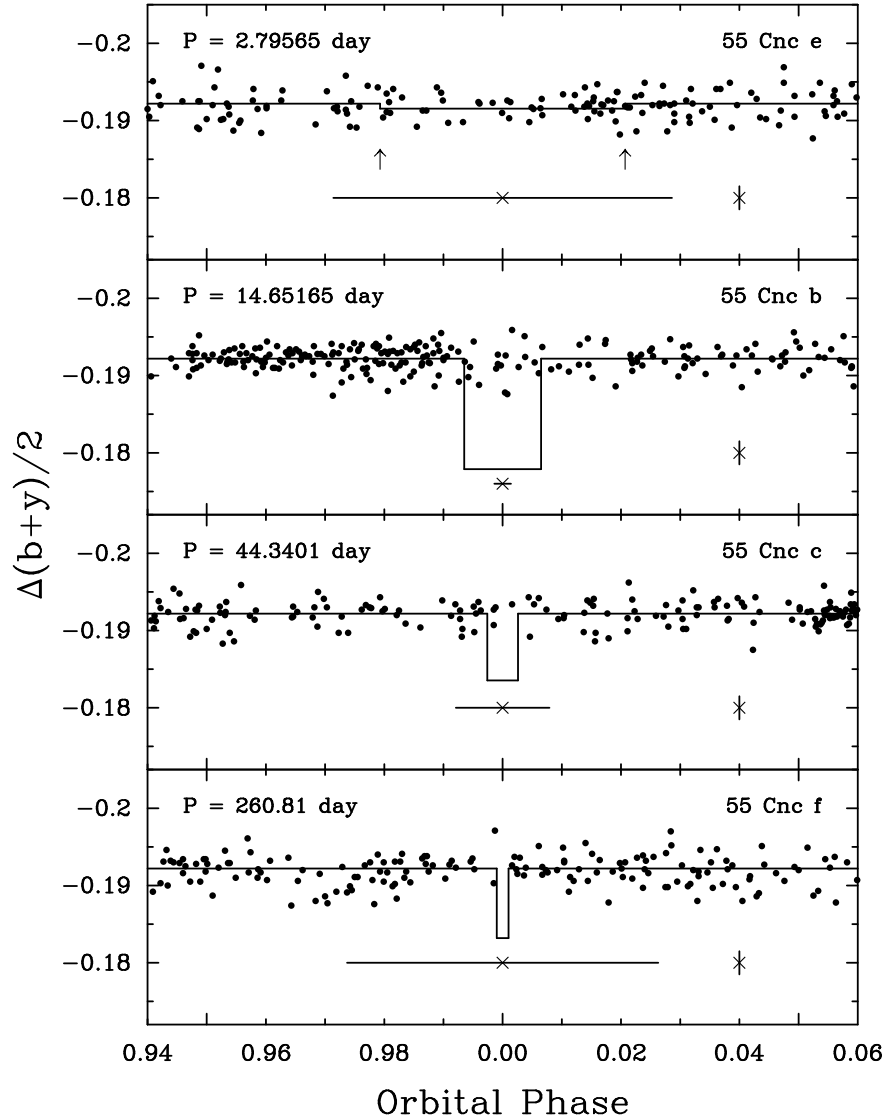
Fig. 12.— Photometric observations of 55 Cnc plotted vs. orbital phase for the inner four planetary companions, all plotted to the same scale. The solid line in each panel approximates the predicted transit light curve, including the depth, duration, and timing of the transits. The arrows in the top panel indicate the beginning and end of the very shallow predicted transits of the inner planet. The horizontal error bar beneath each transit box indicates the uncertainty in the time of transit, while the vertical error bar shows the nominal precision of a single data point. The phase-folded photometry does not detect transits for any of the four inner planets.